Department of Precision and Microsystems Engineering

DESIGN AND VALIDATION OF UNGROUNDED WRIST PERTURBATOR BASED ON PARALLEL MECHANISM

ROBBERT KOENE

Report no : 2022.015
Coach : Dr.ir. V. van der Wijk
Professor : Prof.dr.ir. J.L. Herder
Specialisation : MSD
Type of report : Thesis
Date : 09-05-2022

TU Delft Delft University of Technology

Challenge the future

Contents

1 Introduction

This master thesis came to be as a cohesion project between High-Tech Engineering (HTE) and BioMechanical Design (BMD). The Schouderlab of BMD is well-equipped with a multitude of test setups designed to perform measurements to the human limbs. Their main use is to perform system identification by means of a force or position perturbation. However, the current setups are bulky and bound to the restrictive laboratory environment. This poses a problem with new fields of research that require measurements during daily life. An example study is one that researches the intricate behaviour of arm muscles and reflexes during different tasks. As a human we are able to change the compliance of the arm depending on the different tasks we perform. With assistive robotics becoming increasingly present in current society, we want to quantify this behaviour and implement it into the control of these robots, making them more human-like. To support these types of research during daily life activity, a wearable perturbator must be developed. This device must have the same functionality as traditional devices, i.e. provide perturbations for system identification, but without intruding the freedom of movement of the user. The goal of this project is to analyse, design, and test this perturbator. An assignment that includes combining kinematics and dynamics, precision mechanisms and mechatronics.

The report is split up into four parts. The first of which is the literature survey. While the literature survey is seen as a separate assignment next to the main research, it can be used as a preparation for the final thesis. Therefore, a study was done into the state-of-the-art devices that already exist for ungrounded perturbations, to build on this knowledge and improve on their main flaws. The research question was defined as: "Which actuator principles, from state-of-the-art solutions, are the most promising to generate perturbations for ungrounded mechanical arm impedance measurements?". First, a set of criteria was generated. These criteria were chosen such, that they judged according to the envisioned specifications of the final product. The main body of this research consists of reviewing the current solutions, making an overview table of the specifications, and discussing the main advantages and flaws. Finally, a conclusion was drawn and a recommendation could be made for the most suitable actuator principle for our goals.

Next, the work done during the thesis period is presented in paper format. The goal of the paper was to present a proof-of-concept mechatronic system that is designed to generate controlled force perturbations in three degrees-of-freedom. First, the devised parallel mechanism and servo actuator together with their main properties are discussed. Reasoning on how these are integrated is presented next, together with the CAD of the final design. For validation, a prototype was built and its performance was tested. The results of these experiments are presented and provide ample material for discussion. Features and flaws give insight and recommendations for future research. A conclusion on the viability

of the proof-of-concept is given last.

The last sections of this report include the discussion and conclusion. Unlike the discussion and conclusion of the literature survey and paper, here the whole process will be discussed as one. A study was done into the existing ungrounded perturbators, and the outcome of the thesis research generated another device that can be added to this list. With that, the results can be compared, both to the initial goals and state-of-the-art literature. The final step includes looking back at what is achieved and discuss the scientific relevance, both in the scope of this research and in other scientific fields.

The paper is meant to solely present the final results of the thesis research. The appendix provides background information that might be useful to recreate or improve upon this research. A closer look is taken at the conceptual design decisions and initial simulations and calculations. Details on the first iteration provides insight into the reasoning behind the features of the final design. Furthermore, experimental setups and results are discussed in more detail.

Literature Survey

A study into the suitability of different actuation principles for an ungrounded mechanical arm impedance measurement device.

Robbert Koene

4497902

MSc High-Tech Engineering

Delft University of Technology

Contents

1 Introduction

From the field of BioMechanical Engineering there is a great interest in measuring the mechanical properties of the human body. An accurate model of the human arm provides the basis for many other fields to base their research on. Within the field of robotics, this data can be used to make robots in healthcare more human-like [24]. An example of a medical application is to see the progress during rehabilitation of stroke patients [19].

The common way to model a human limb is by defining mass (inertia), stiffness and damping properties [1]. Measuring these parameters is done via system identification. System identification is a methodology to build a mathematical model by measuring a systems output as a results of a known input over time [18]. Traditionally, a test subject receives a positional perturbation by a grounded mechatronic device. An example of this research is the work by Mugge [23], who researched sensory weighting of force and position feedback in human motor control tasks and Hondori [21] who researched the real and imaginary parts of human arm mechanical impedance. Depending on the goal of the research, this method can provide accurate and repeatable results. However, these fixed setups have their limitations that make them less suitable for studies on daily life movement.

The mechanical properties of the human arm are task dependent [22]. Performing a reaching task in an unknown environment requires low impedance, the body reacts by relaxing the arm muscles. The contraction of the antagonist muscle, in turn, results in a higher arm stiffness, necessary when resisting perturbations during lifting of heavy objects. Impedance control makes use of this variation in stiffness and is already being applied to the field of robotics and medical prostheses [16] ; [8]. Especially in these fields of research, impedance data of human limbs during daily tasks is most useful. With current grounded solutions, the test subject is bound to a lab environment with intrusive machinery. Furthermore, the position perturbation imposed by the manipulator stabilizes the movement of the limb, since its stiffness is much higher. To gather insightful data outside the lab, new devices for measuring mechanical arm impedance are necessary.

In recent studies, multiple solutions have been researched to perform ungrounded measurements. These solutions replace the device connected to a rigid base that provides a positional perturbation, with a portable device that provides force perturbation. An accurate measurement of the force signal together with the resulting limb displacement provides the data to perform system identification. The actuation principles range from inertial accelerations (e.g. [4]) to pneumatic pulses (e.g. [15]). However, not only biomechanical devices provide the ungrounded perturbations necessary to perform system identification. In other fields, like that of virtual reality, a lot of work has been done on force feedback to create a more immersive experience (e.g. [6]).

As for generating an ungrounded perturbation within the field of biomechanics and beyond, no actuation principle seems to be dominantly present. Therefore, the research question for this literature review is formulated as follows: ‘’Which actuator principles, from state-of-the-art solutions, are the most promising to generate perturbations for ungrounded mechanical arm impedance measurements?” To answer this question, a number of criteria important for ungrounded impedance measurements will be drawn up. Based on this, performance data of actuators from different perturbation devices are compared. Certain characteristics that inherently belong to the different actuators will also be mentioned.

2 Criteria generation

The first few criteria are related to the perturbation properties that belong to the actuation principle. An ungrounded disturbance can be either introduced by a force or a torque. The respective possible magnitude and degree-of-freedom of these need to be assessed. Depending on the measurement resolution and frequency, the output data (displacement/acceleration) is required to have an adequate signal to noise ratio. To generate valuable data for research, the actuation principles also need to be graded on repeatability.

The bandwidth of an actuation principle determines the possible system identification methods. These range from a single transient pulse to a high frequency stochastic signal [18]. The duration of a pulse is bound by the response time of the shoulder reflex arc, which is approximately 25 ms [14]. If the signal remains below the response time, intrinsic muscle-tendon stiffness can be measured. A longer pulse introduces positional feedback of the central nervous system, resulting in the measurement of reflexive stiffness. To see which identification methods can be applied, the bandwidth and response time of the actuators are assessed.

While measuring mechanical impedance properties of the arm, the mass of the actuator (the device) is to be kept ass low as possible, since it changes inertial properties. This is important for both for model accuracy and comfort during operation. A state-of-the-art device that offers high perturbing forces while being heavy, might be suitable for down-scaling. Therefore, the force-to-weight ratio is adopted as criterion.

Next to mass, some other properties that inherently come with certain actuating principles can also influence measurements. Like the gyroscopic effect of fast spinning bodies. While gyroscopes can be used to stabilize movements [28], this effect will negatively influence the outcome of the experience. Also the dynamic properties (e.g. resonance) of the actuator itself can be of influence [18].

A criterion that is harder to quantify, but therefore not less important, is intrusiveness of the actuator solution. A bulky device will limit the freedom of movement and interfere with daily tasks. Mechanical arm impedance measurements are susceptible to human emotions [20]. Experimental results will differ when a person is stressed or spooked by the device. Sudden loud or harsh sounds, large vibrations or physical discomfort during operation are examples of factors that can influence the outcome of the experiment. The actuators and all other auxiliary equipment needed to drive the actuator will therefore be graded on intrusiveness.

3 State-of-the-art

3.1 Pneumatic

Höppner [15] agrees that positional disturbances with devices that are fixed to the world, limit the freedom of movement during impedance measurements. Therefore, he developed a wearable pneumatic solution that relies on force perturbations.

The force perturbations are generated by accelerating and decelerating a mass (piston) within the pneumatic cylinder with air pressures ranging from 3-5 bars. Höppner has decided to focus on measuring the intrinsic muscle-tendon stiffness of the arm, introducing the pulse limitation of 25ms. Modal analysis can be done on the arm by applying oscillatory force perturbations, however this requires multiple disturbances within 25ms. This is deemed impossible by Höppner, due to the compressibility of air and resulting time it takes to build up sufficient pressure. The transient force that can be generated within this 25ms window is simulated (and validated) to be around 1300N. However, the physical effect of this force on the human arm, a measurable displacement/acceleration, was not included in this research.

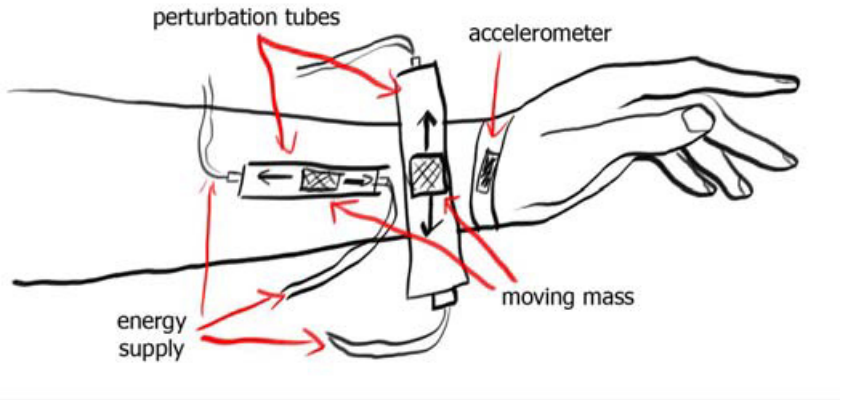

Figure 3.1: Sketched overview of the system

The number of cylinders and the respective alignment determines the amount of DoF in which the system can measure. For purely transnational movements, two cylinders per DoF are necessary. The cylinder can be operated bidirectionally by switching valves. A smart design suggestion was made by Höppner to increase acceleration and mitigate some of the effects of a compressible fluid. A magnet could be installed in the cylinder stops, so that first the pressure must increase to such extent that the magnetic attraction force is overcome. However, this is not actually applied to the prototype.

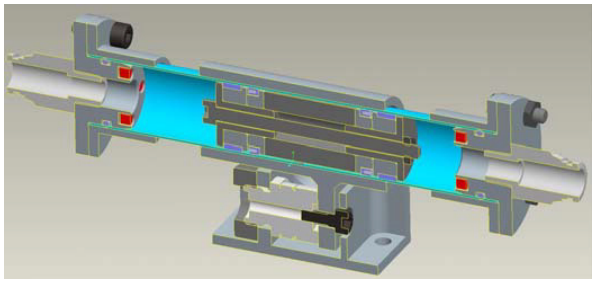

Figure 3.2: CAD design

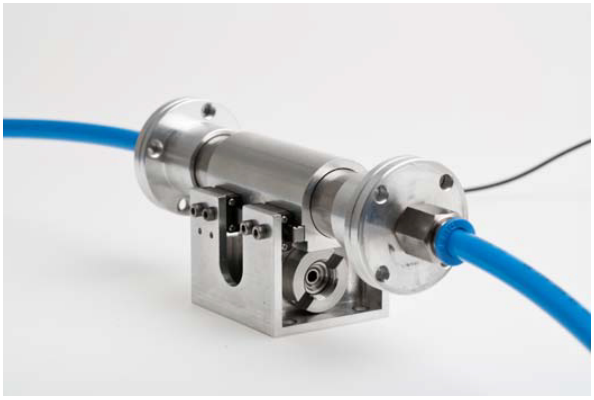

Figure 3.3: Prototype test setup

The device is tested on a test bench and the performance is analysed using an acceleration sensor with a sampling rate up to 10kHz. The exerted force is measured with the actuation time. The peak force of 1300N is a results of the piston colliding with the end of the cylinder. The perturbation lasts for 14ms.

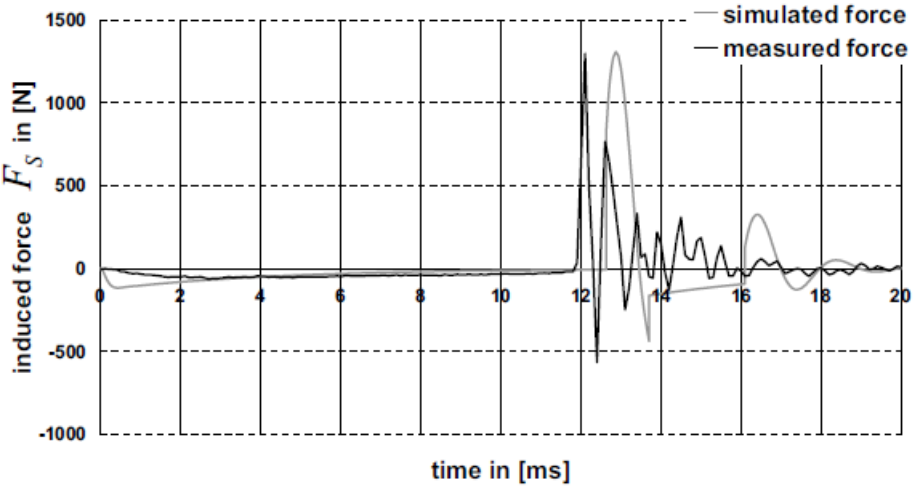

Figure 3.4: Test results, simulated vs measured force

The above shown result indicates a similar profile between the simulated force and the measured one. Peak forces are corresponding, however the simulated reaction time and overall time between stops is less accurate. Höppner links this to the unpredictability of the friction coefficient (stick-slip) and the difference between a real and an ideal air reservoir. He also noted the influence of tubing length, piston mass and air pressure on the response time and kinetic energy of the system.

While the initial maximum weight was set to be 500g, the weight of the final prototype was not stated. One can estimate that a pure translational multi-DoF system with this actuation principle is both bulky and heavy. However, since the system provides a perturbation of 1300N, a downscaled

mechanism would still suffice for impedance measurements. Moreover, the pneumatic tubing that runs to the device, can be considered to be intruding. Another factor to consider is the need for auxiliary components to drive this system, such as a pressure tank, regulator, and valves.

Related to the work of Höppner are other pneumatic solutions which are based on a different working principle. An example is the work of Xu [34]. He developed an airjet perturbator that provides high-frequency perturbations to the wrist in three orthoganol directions. This system has some very promising properties, a steady state thrust of 4N, stable up until a bandwith of 75Hz, operating at 80 psi (5.5 bar).

Xu describes how most state-of-the-art systems use electric motors, because of readily available components and accurate position transducers to measure the rotor motion. However, he states that electric motors are bulky, have a relatively low force to mass ratio and are unable to generate high frequency perturbations due to high rotor inertia. Another option considered by Xu are hydraulic actuators. Even small sized hydraulic actuators are able to provide high forces at a very high bandwidth. However, both electric and hydraulic solutions are assumed to be harder to implement in a multiple DoF system, although not impossible. Rods or cables could provide the desired DoF's, but introduce more complex dynamics and will most likely reduce the perturbation bandwidth.

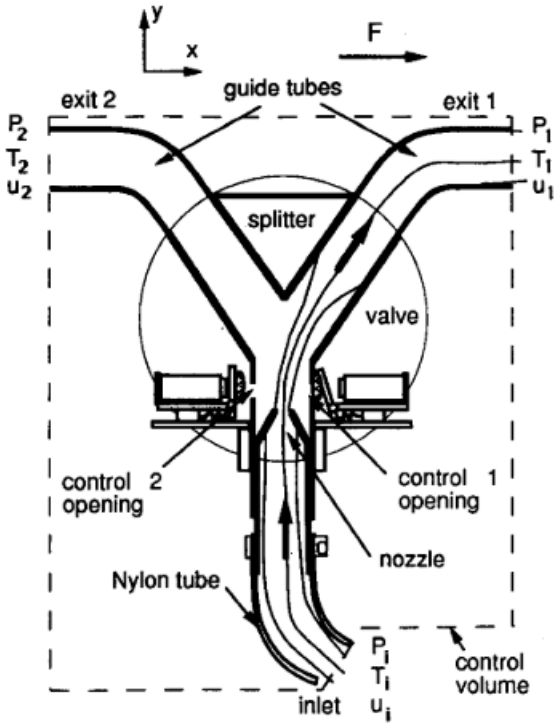

Figure 3.5: Novel valve design that allows for a high switching frequency

Since Xu states that high frequency stochastic perturbations are best for identifying the mechanical properties of the arm, he opted for a pneumatic airject system. Existing air jet systems did not meet his

requirements for bandwidth, having a maximal frequency of around 20Hz. The bandwidth of then state-of-the-art systems were limited by the switching frequency of the valves. A new design was proposed with a fluidic switching device that is based on the Coanda effect. The system is designed to generate arbitrary binary force signals, such as pseudorandom binary sequences, colored white noise, and Walsh functions. A three-dimensional optical tracking system was used for motion tracking. The natural frequency properties of the human arm, together with the accuracy of the motion tracking provided the requirements of the system to have a force perturbation of 4N at a frequency of 100Hz (PRBS signal).

Xu has no pure translations and his method of attaching the actuator to the arm results in a bulky intrusive system. However, these problems can be solved with a different implementation of the air jet system. The actuation principle of air jets is promising in terms of force generation and bandwidth. One can assume that the sound of the gas being purged from the nozzle can be harsh and therefore influence the measurement.

Belden [7] continued on the design of Xu and made lightweight (0.075kg) prototype using 3D printing. A test setup with mass-spring-damper-system was constructed. After static force calibration, linear stochastic system identification experiments were performed and with that the functioning of the system was validated. During the experiments the bandwidth of the pseudo-random binary signal was limited to 10Hz by the switching solenoid. The signal and resulting displacements that were used to perform system identification is shown in Figure 3.6.

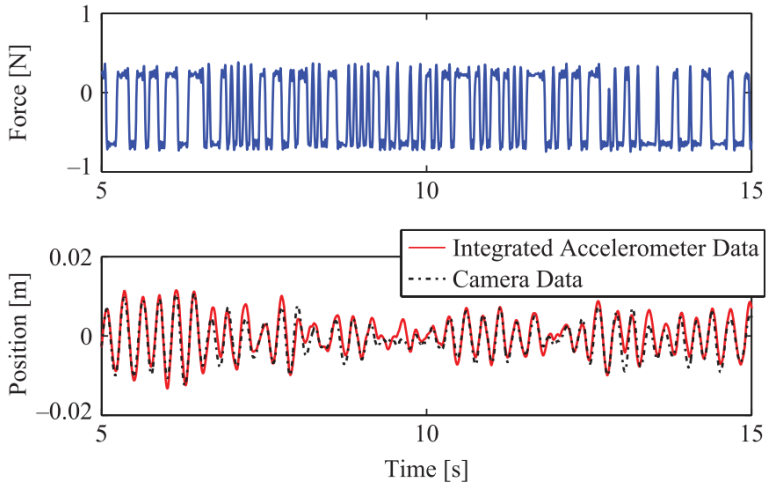

Figure 3.6: Perturbation signal with corresponding displacements

The outcome of the system identification is a second-order model with which the systems response can be predicted. Belden validated his work by testing his models against the real world response of the system. The results of this experiment are shown in Figure 3.7. The displacement is measured by both a camera and an accelerometer, and a model is made with each one respectively. Both models provide

an excellent prediction of the real world displacement.

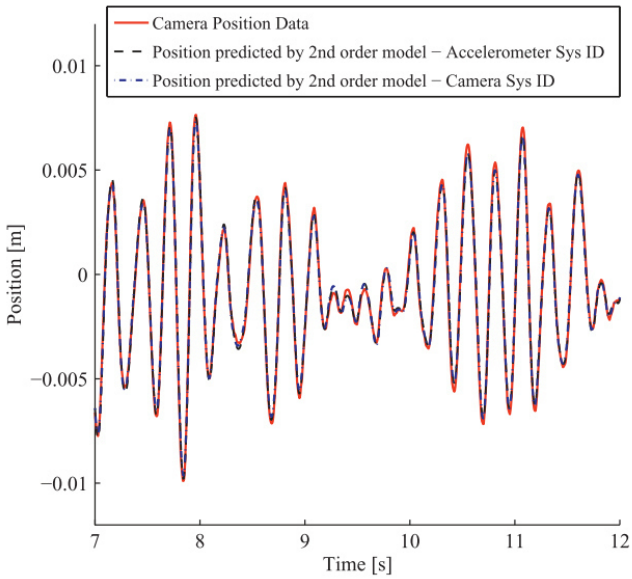

Figure 3.7: Real world displacements vs modelled movement (dashed)

The proposed designs of Höppner, Xu, and Belden all provide a 1DoF perturbation. However, all three recognize the possibilities to expand their systems to multiple DoF. Gurocak [12] has implemented six pneumatic ports in the three Cartesian directions on a wrist mounted design (Figure 3.8). Allowing his system, which is designed to provide weight sensation for VR, to generate 3DoF perturbations. The airjet actuation principle resembles that of Xu and Belden, however nozzle and valve designs are less sophisticated. Switching between the ports is done by more traditional servo valves, with are placed externally together with the air reservoir.

Multiple nozzles can be opened at once, resulting in an arbitrary force direction. However, since all nozzles have the same air reservoir, the provided pressure and thrust has to be controlled when blowing through multiple nozzles. Gurocak implemented a PI controller to reject these disturbances within the air pressure. The maximum force and bandwidth were evaluated experimentally to be 7.3N and 15Hz respectively. Since this system is developed to simulate weight sensation in VR, there is no experimental data on signals for system identification. However, since the actuation principle is similar to that of Xu and Höppner, a PRBS signal at 15Hz is assumed possible.

The mass of the device is unknown, but since the passive box only houses six nozzles, it can be assumed a lightweight solution. The decision to keep the wrist mounted device lightweight comes at a cost. The direction of the pulse is controlled by external valves, resulting in six individual pneumatic hoses running along the users arm. This dramatically reduces the freedom of movement.

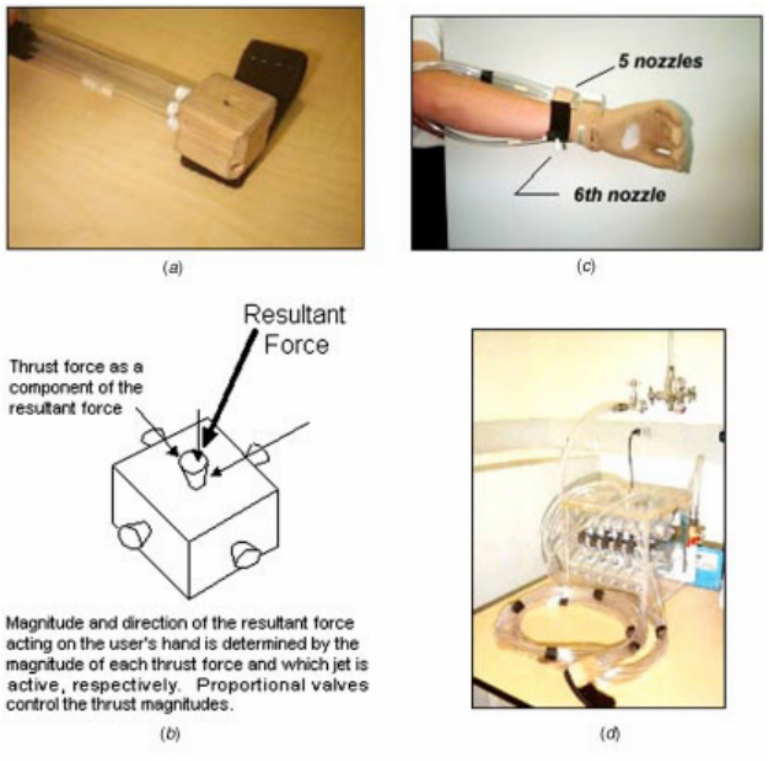

Figure 3.8: (a) Air jet block, (b) concept prototype (c) placement of the sixth port (d) remote box

3.2 Electromagnetic

3.2.1 Rotational

There are multiple ways to generate an ungrounded torque perturbation (Figure 3.9). First, we will discuss the method of perturbing with an asymmetric torque (option (b) in Figure 3.9). Both Amemiya [3] and Choinière [9] designed a 1DoF haptic compass using this technique. The devices, consisting of a flywheel and one or more DC motors (Figure 3.11), have a simple design but are able to generate repeatable results. Both weigh approximately 0.35kg and the torque perturbation is scalable in these kind of devices by altering the inertia of the flywheel.

A brushless motor generates torque pulses in alternating directions by accelerating the inertia of the motors rotor and external mass. To make the signal asymmetric, the pulse consists of a ”haptic” torque and the ”recovery washout” torque, as can be seen in Figure 3.11. During the calibration of the device, the dynamic properties were studied and with open-loop control Choinière was able to get accurate results. Resulting in the following performance paramters of his device; a bandwidth of 50 Hz and a maximum torque of 100 Nmm. The duration of the perturbation can be extended to a maximum of 0.5 seconds. Choinière mentioned that, during these short pulses already, the gyroscopic effect and

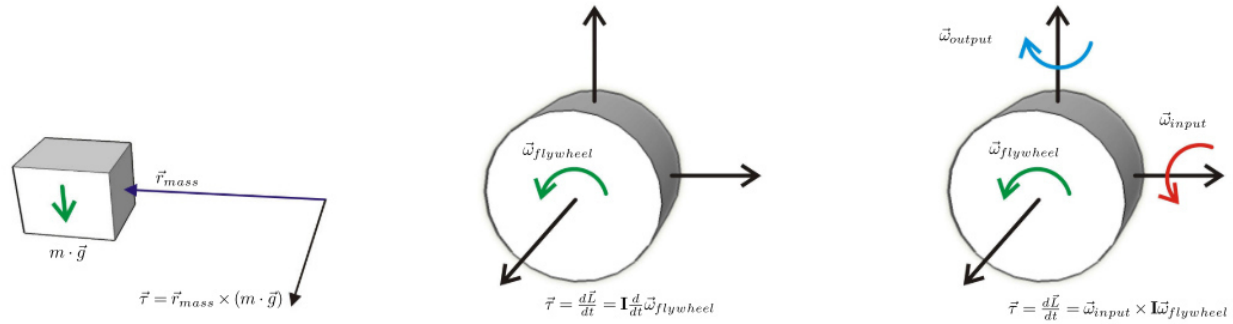

(a) Force at a distance (b) Momentum wheel (c) Steered momentum wheel

Figure 3.9: Three ways to generate an ungrounded torque according to Winfree (2009)

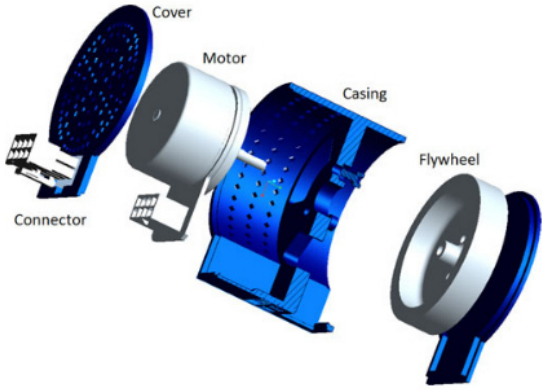

Figure 3.10: Exploded view of asymmetric torque perturbation device

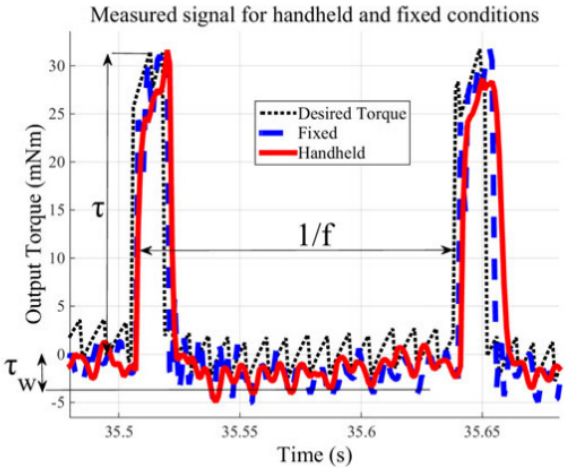

Figure 3.11: Torque signal induced by flywheel

vibrations were noticable while performing the tests.

Hondori [22] had the goal to design a simple yet reliable tool for the assessment of motor function. The 'Smart Mug' is a hend-held device that uses an eccentric mass driven by a DC motor to generate a continuous sinusoidal signal. At 10Hz and a mass of 0.1kg, the centrifugal force is roughly 7N. During the experiments, a two-axis inertial sensor measured the arms accelerations as a result of the perturbing forces. With his device he was able to conclude that mechanical impedance is posture dependant.

Another way to generate ungrounded perturbations using rotating bodies, is with the gyroscopic effect. Here, the principle of conservation of angular momentum is used. In multiple scientific papers a fast spinning flywheel, supported by a pan-tilt (gimbal) mechanism with two servo motors, is rotated to generate a perturbing torque.

Yano [32] has developed such a device. A single flywheel spinning at 8000 rpm generates torques

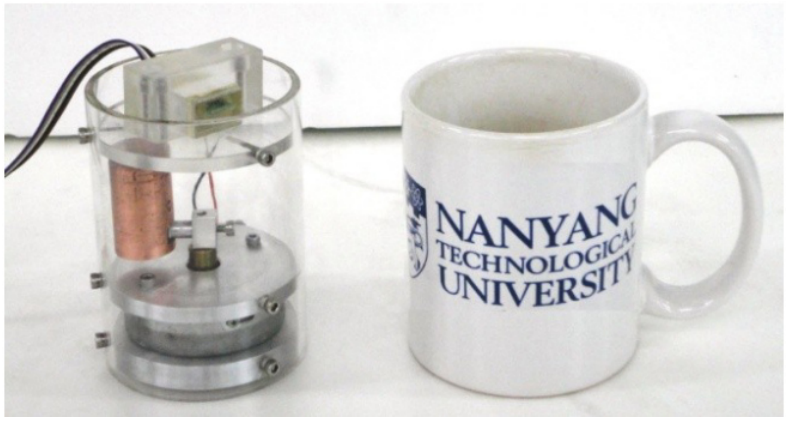

Figure 3.12: Smart Mug, an ergonomic hand-held design to measure arm impedance

in arbitrary directions (3DoF). His device can provide a transient disturbing torque of 118Nm, while weighing 650 grams.

In his discussion, Yano mentiones that the prototype has its limitations with respect to the tilt angle and also requires a washout time to return the flywheel to its original direction. Those problems cause a short signal duration time and a low bandwidth torque perturbation. Furthermore, to generate torque with a flywheel, you generate a perpendicular reaction torque to turn the flywheel (no pure torques). This reaction torque is proportional to the generated torque. Yano did an experiment with his device (Figure 3.13), showing this relationship. A slight deviating from a linear relationship can be seen due to friction. Due to the servo motors limited torque, saturation occurs at around 2000 gfcm.

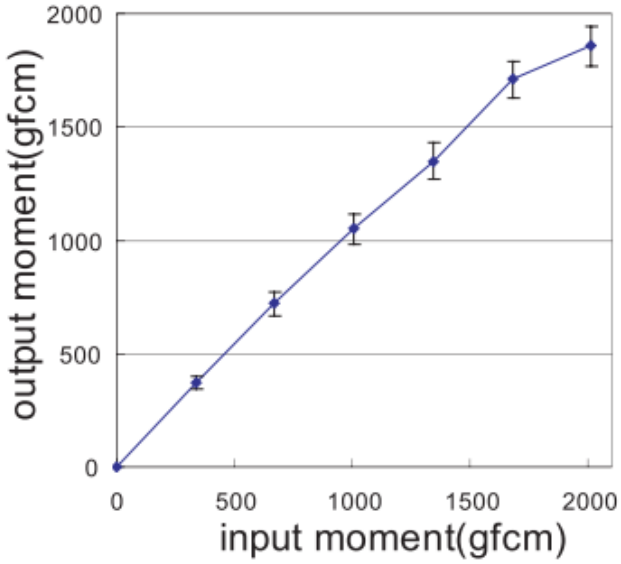

Figure 3.13: Relation between input and output torque for single flywheel actuator

Winfree [31] also developed a device, giving the user the impression that their hand is being twisted in free air. This prototype was able to generate up to 1.2Nm of torque. However, no experiments were done on the bandwidth/time constant of the system. Components and materials were carefully chosen, which results in a relatively lightweight two-axis gyroscopic system at 486 grams.

The operational principle is very similar to that of Yano. However, in stead of using readily available servo motors (like used in the other papers mentioned), Winfree has chosen for a DC motor with a cable drive to control the two-axis rotation of the flywheel. This is because a servo motor has the positional feedback and the internal gearing has a lot of friction. Since flywheels have a tendency to remain in a steady direction of its axis of rotation, the ”stiffness” of the servo motor results in continues reactive torques while moving around the device. The solution chosen by Winfree allows the flywheel to remain in its original direction, while the user is rotating the device. Therefore, only imposing torque perturbations when desired.

Winfree also notices that small hobby grade motors at high rpm generate a lot of vibrations. And since a low mass flywheel at high rpm can be replaced by a higher mass at lower rpm, this is in some cases desirable.

Implementing a dual flywheel setup enables the reaction moments created by two flywheels spinning in opposite directions to be cancelled, leaving only the desired moment about an arbitrary axis. Walker [29];[30] did extensive research on this solution (Figure 3.14 & 3.15).

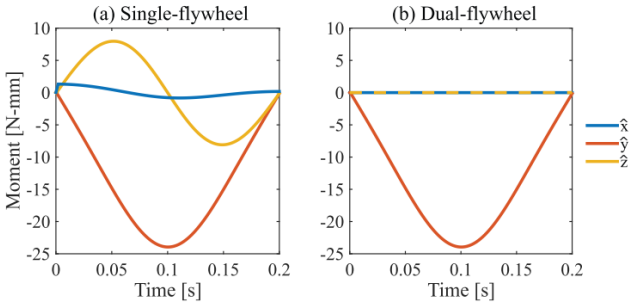

Figure 3.14: Theoretical example of moment cancelling with dual flywheel

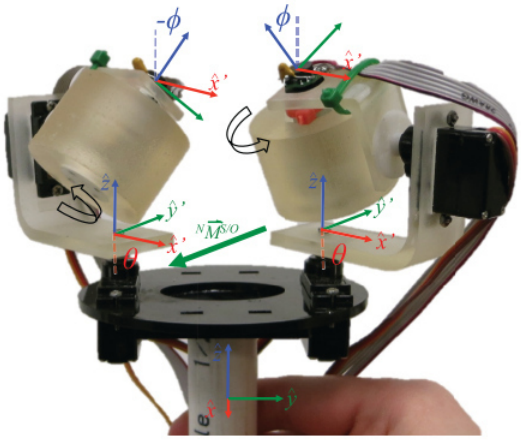

Figure 3.15: Dual flywheel prototype

The prototype consists of two flywheels supported on a gimbal mechanism, each with two servo motors. The lower servo motor is rotated first, to get the desired torque direction. Then the upper gimbals were rotated in opposite directions to generate the moment pulses. This results in a 3DoF system with torque perturbations in arbitrary directions. In Walkers research the torque perturbations were generated at a frequency of 1.25 Hz. Each strong pulse was 200 ms long and each weaker return pulse was 600 ms (Figure3.16). The flywheels are rotated at a speed of 1500 rpm. The torque of 25

Nmm was limited by the performance of the servo motors.

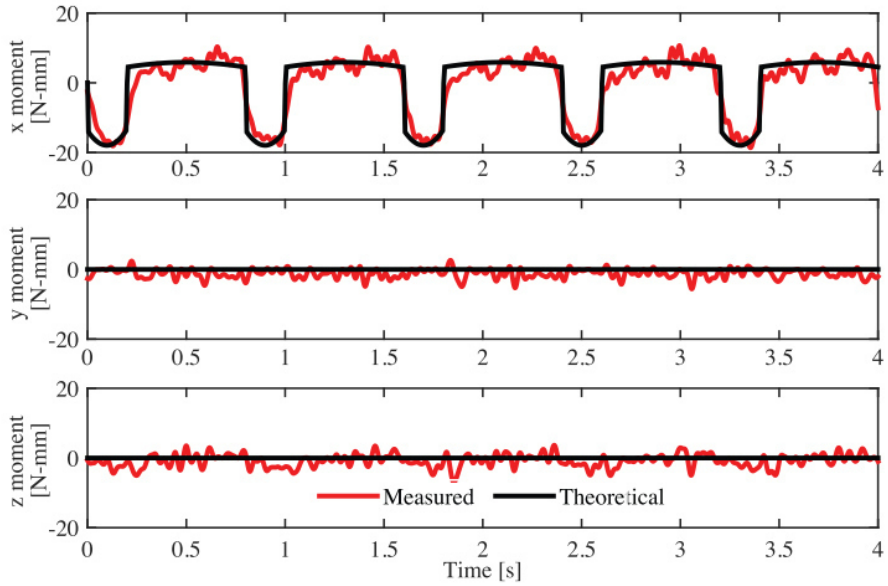

Figure 3.16: Torque perturbation in one direction, without reaction torques in the other directions

Two years after publishing the first paper, Walker improved upon the old design. This prototype, again, had two opposing gimbals to counter the reaction torques. The flywheels were placed in a new orientation, and with stronger servos the peak torque was increased to 51.2 Nmm, while the weight was slimmed down to 197.7 grams.

3.2.2 Translational

This section discusses electric actuation principles that generate translational forces in a certain direction. Culbertson [10] and Tanabe [27], for example, both designed a hand held ungrounded haptic interface that generates an asymmetric vibration signal. The idea is that the asymmetry causes either a pushing or pulling sensation on the skin. The actuators used are off-the-shelf voice coils / vibration speakers, which working principle both rely on an electromagnetic field created by a coil. These solutions are lightweight and simple to control.

Both setups have dual actuators, which when used in phase double the force and when used in antiphase can generate a torque. At a frequency of 75Hz Tanabes device generates a maximum force perturbation of 1N. At 100Hz, when in resonance, Culbertsons solution generates a 5N perturbation.

Kakuda [17] designed multiple iterations of a cam mechanism to generate ungrounded forces. It works based on a rotating cam that periodically accelerates a mass, resulting in a 1DoF force perturbation. In the last iteration, Kakuda made a grooved cam, where the mass follows the cam profile accurately. At the tip of the cam, there is a discontinuity in the position in x-direction, this is how

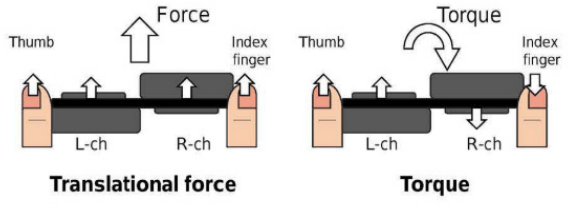

Figure 3.17: Two vibrational speakers able to generate both forces and torques

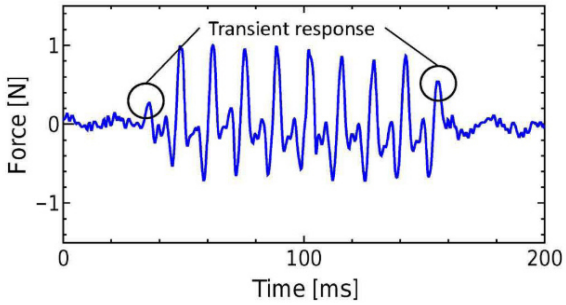

Figure 3.18: Force signal of vibrational speakers

the asymmetric acceleration is generated. However, this also results in an undesired vibration in y-direction. Smoothing the cam profile reduces this vibration, but also the (force) performance of the device.

Although the goal of the paper was not to create the highest possible perturbation force, it still resulted in around 25N. The frequency (or motor rpm) at which this force was generated was not mentioned, but experiments with volunteers testing the force perceptions have been done at 10Hz. Weight also is not mentioned, however it does seem to be quite a large device for generating a 1DoF perturbation

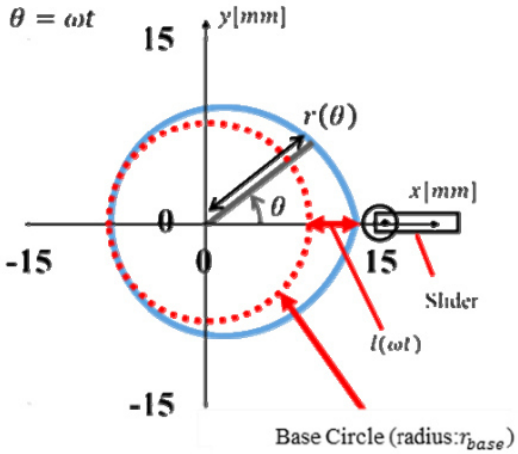

Figure 3.19: Cam design of Kakudas device

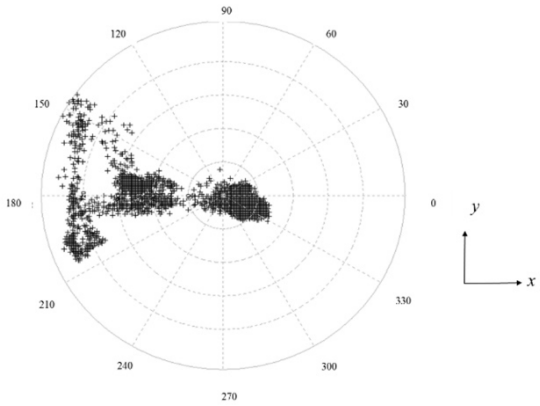

Figure 3.20: Force direction and magnitude of cam mechanism, outer ring representing 25N

Amemiya [2] uses a crank slider mechanism to generate a virtual force vector for wayfinding (Figure 3.21). The rotary movement of an electric motor is converted to a rectilinear movement. The mechanism is designed to maximize asymmetric accelerations of the moving mass. The signal is periodic, with a large quick pulse of acceleration followed by longer low-amplitude recovery. The mechanism also generates an acceleration signal in orthogonal direction (Figure 3.22). For our intended purposes, this is unwanted behaviour. However, since this the device is designed to give the user a virtual force

perception in a certain direction, it is less of a concern. The experiments are therefore focused on evaluating how well the user can discern the direction of force, with varying motor speeds and moving mass. It can at least be concluded that the device, with a weight of 230g and a moving mass of 20g, can generate 17.5N at 10Hz. In later research [5], Amemiya wanted to make the pulling/pushing sensation of the device more effective. By adding a mirrored version of the mechanism, he managed to cancel out the orthogonal parasitic accelerations.

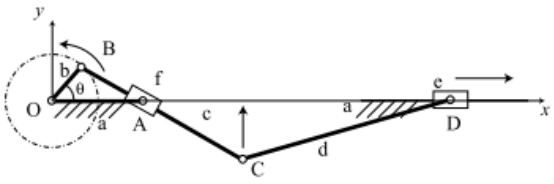

Figure 3.21: Schematic overview of the crank slider system

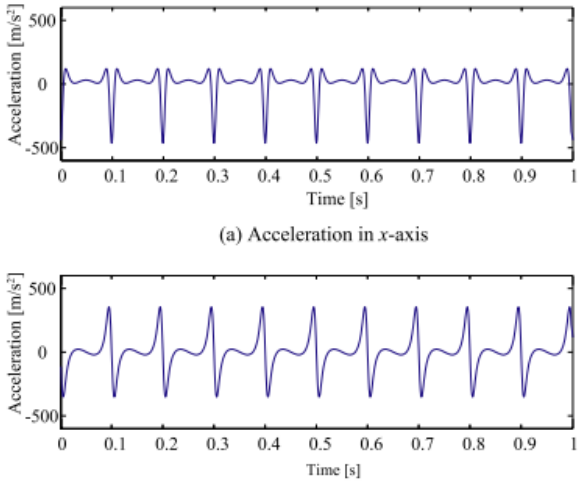

Figure 3.22: Acceleration being generated in two directions

Hamaguchi [13] wanted to achieve the same ungrounded force sensation. In the paper, this is achieved by two rotating masses that periodically hit a wall. The resulting signal is an asymmetric force perturbation. Here, a large force spike is generated when the masses hit, and a longer smaller force occurs as the masses increase speed again for the next hit. Since the masses spin in opposite directions, a pure 1DoF force is generated (Figure 3.24). The material that is being hit by the rotating masses, was varied. By varying this, and parameters like the size of the weights and motor speed, one is able to tune the signal shape. While again, testing the force sensation of the user was the main goal of the experiments, we can derive some important device parameters. The maximum force produced is 24N, with an impact frequency of 5Hz. The length of the pulse is 30ms. The device is quite bulky as it is mounted on a plate, weighing around 420g (Figure 3.23).

Shima [26], like Hamaguchi, makes use of periodic knocking to generate an asymmetric force perturbation. However, this time it is based on a mass-spring-system (Figure 3.25). The system makes use of resonance and is excited by a voice coil motor. The system is tuned to have a resonance frequency at 10Hz. The resulting signal is the force generated by the impact, lasting 3ms and the reaction force of the motor (Figure 3.26). The maximum force generated is 28.6N. The weight of the device is 230g, a part of which can be accounted to the linear guidance needed for the moving mass.

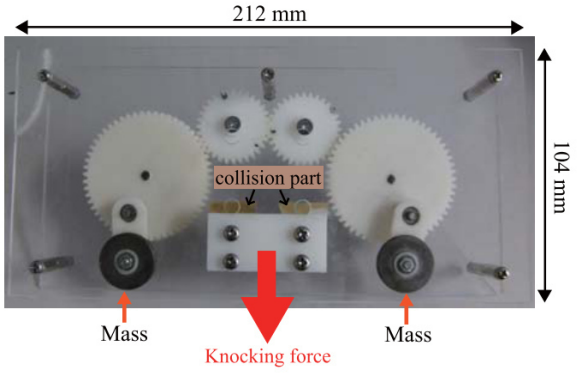

Figure 3.23: Knocking principle prototype

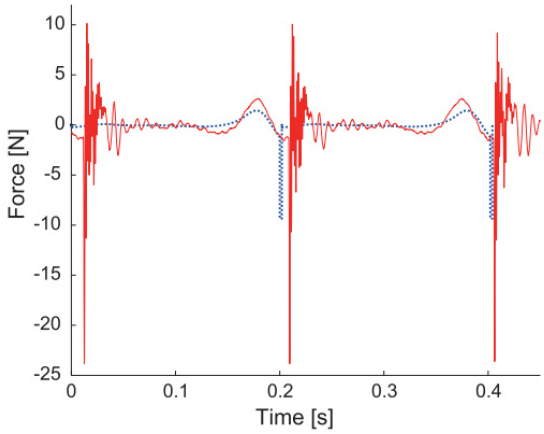

Figure 3.24: Force signal over time

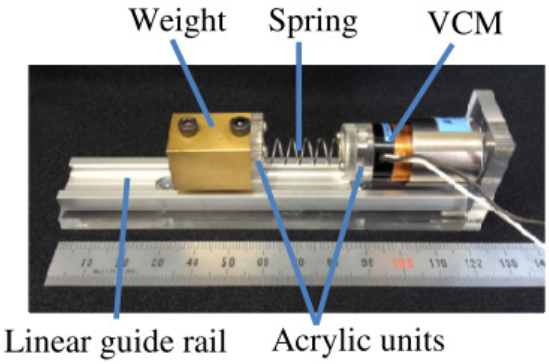

Figure 3.25: Design of periodic knocking device

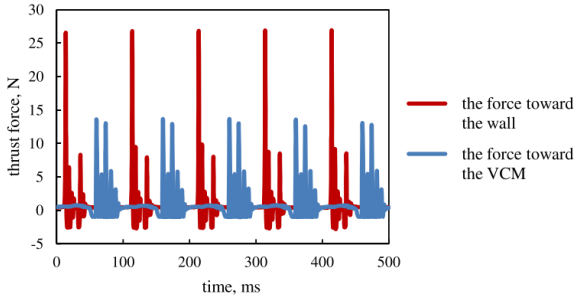

Figure 3.26: Force signal generated by Shimas design

3.3 Piezo

Piezoelectric actuators have certain properties that are interesting when designing a portable perturbation device for human limb system identification. For example, their high bandwidth, force and stiffness, their lack of moving parts while also being compact. However, to the best of my knowledge there are no examples of this kind of actuator being used in mechanical impedance measurement setups. In related fields of research, like force/haptic feedback, there are some examples of tactile ”buzzing” piezoelectric actuators generating high frequency low force signals [33]. These signals are not suitable for our purposes.

One of the few options available to implement a piezoelectric actuator is with the use of a actuator stacking or motion amplifier. An example of this is the haptic interface developed by Sauvet [25]. The device (Figure 3.27) consists of a movable mass guided by a linear rail, an aluminium mechanical structure, and the piezoelectric actuator connecting the two. The total mass adds up to 262 grams.

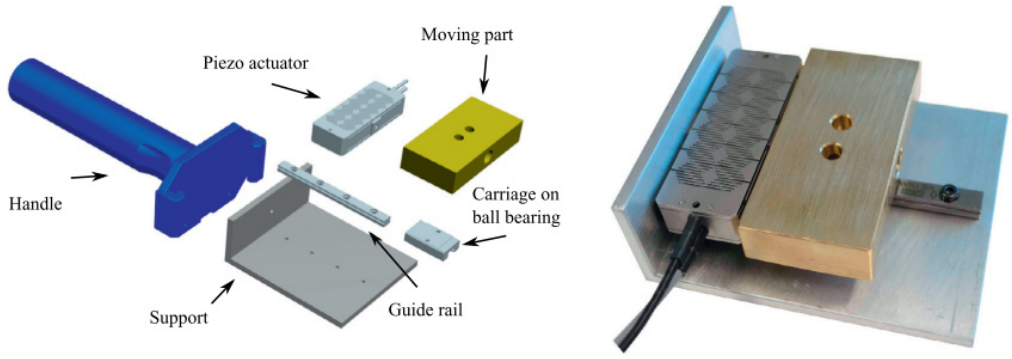

Figure 3.27: CAD design (left) and finished prototype (right)

Since it is made with the purpose of creating a haptic directional perception, the signals are generating asymmetric accelerations. An example of the perturbation signal, with a 200g mass and a frequency of 60Hz, can be seen in Figure 3.28. The device can be considered a mass-spring-damper system when mounted rigidly on a test bench. However, when hand-held it results in a double mass-spring-damper system, because of the added dynamics of your hand/arm. Sauvet suspected that the natural frequency of both the arm and the device would influence of the performance. He therefore experimented with different masses at different frequencies (results shown in Figure 3.29).

Results show that the acceleration of the moving part decreases as its mass is increased. Although the acceleration is decreasing, the force generated is compensated by the increase in mass. From the results we can also conclude that increasing the mass and acceleration frequency both contribute to the force produced by the moving part. Ideally, the moving part should contribute the largest possible percentage of the total mass in order to optimize the performance of the device.

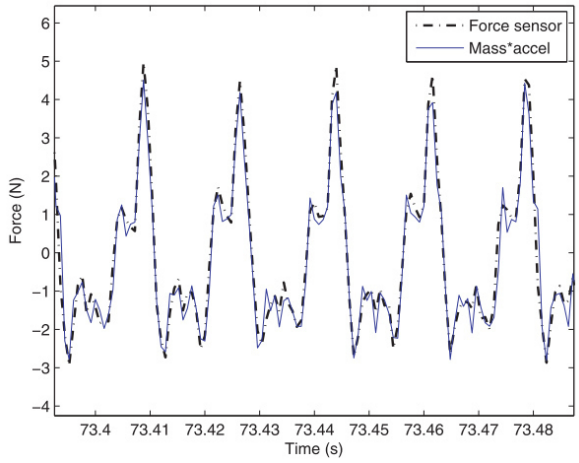

Figure 3.28: Force signal with moving mass of 200 grams at 60Hz

Table 7
Maximum average values of the accelerations and the forces of the moving part. Asterisks (*) represent the values measured by a sensor. Values are calculated from the average of 220 samples.

Acc freq (Hz)	40	50	60	70	
No mass added	12.7	19.3	24.1	25.3	m/s^2
	1.77	2.68	3.36	3.53	N
100 g added	10.5	13.8	16.7	17.5	m/s^{2*}
	2.50	3.30	3.99	4.18	N
200 g added	8.38	11.6	14.3	14.6	m/s^{2*}
	2.84	3.92	4.84	4.96	N
500 g added	6.6	9.41	11.2	11.6	m/s^{2*}
	4.22	6.01	7.13	7.43	N

Figure 3.29: Influence of different frequency and mass combinations on the generated force

Sauvet also concludes that the optimal perception frequency is very close to that of one of the

resonant frequencies of the device. Optimal perception can be translated to the extent in which the arm in perturbed, which is interesting for our current research. From his experiments Sauvet also shows that the value of the resonant frequency is user dependent. This means that, to get optimal performance from this actuation setup, the mass and frequency have to be tuned per user.

4 Review

4.1 Pneumatic

Four different papers on pneumatic solutions for creating an ungrounded perturbation are reviewed. Two main operating principles can be distinguished; accelerating mass (piston) and airjet. There are multiple general advantageous properties of pneumatic solutions that apply to both principles. The main reason for deciding on a pneumatic system might be their relatively high force to weight ratio (see Table below). High pressure air supply and the auxiliary electronics can be mounted externally, making the device simple and lightweight. The control of a pneumatic system is more straight-forward than electromechanical solutions. The magnitude of the perturbation is easily scalable by changing the operating pressure. Finally, increasing the number of degrees-of-freedom is done by simply adding nozzles/cylinders.

A downside of both pneumatic principles is the need for a high pressure air supply. A small disposable gas cartridge, as proposed by Belden, can provide a portable solution. However, all prototypes discussed still rely on a fixed pressure supply. To direct the airflow, electromagnetic valves were the obvious choice. When mounted externally, two air lines have to run along the arm per degree of freedom. When implemented in the device and combined with the Coanda effect, the number of air lines is halved. However, the valve does increase the weight of the device and its dynamics might introduce parasitic force signals. The necessity for an air supply and air lines decrease the freedom of movement during experiments. Moreover, while using pneumatic devices, the air has to be purged. Either on the device, when considering the airjet principle, or externally. The sound of purging air can influence the experiment in a negative way [20]. Since all experiments in the provided literature are done on a test bench, influence of movement of the test subject is not taken into account. However, one can imagine that pinching of the air lines during movement of the arm can influence the force that is exerted. This can result in posture dependent repeatability of the setup.

The accelerating mass solution, specifically, is able to generate a very large force perturbation, with the highest force-to-weight ratio of all discussed researches. However, the mass (piston) is accelerated by the pressure build-up within the cylinder. Due to the compressibility of air, the achievable bandwidth is limited compared to the airjet solution. Furthermore, the moving piston has a rubber seal, which introduces unpredictable stick-slip behaviour, making accurate modelling and repeatability difficult.

The airjet principle, specifically, is easy to scale up to a lightweight multi degree-of-freedom solution. High bandwidths can be achieved and are limited mainly by the switching frequency of valve.

This solution can offer a large range of signal types. And in contrast to other solutions, the length of the perturbation is adjustable. However, in his research Xu measured noise of 80-110dB with his airjet system, only bearable with ear protection.

4.2 Electronic

The electronic solutions that were researched, can be distinguished by actuation principle and the resulting perturbation. Flywheels are used in many devices, to generate torque pulses by either accelerating (decelerating) them, or using the principle of conservation of angular momentum. The advantage of using a flywheel to generate ungrounded perturbations is its simplicity and robustness. By accelerating the a flywheel, we can obtain a high bandwidth and repeatable 1DoF perturbation. To expand these solutions to mulitple DoF would require multiple flywheels in different directions. Using the principle of conservation of angular moment in 1DoF, always results in a parasitic torque in perpendicular direction. However, with two flywheels mounted on gimbals, Walker was able to generate pure 3DoF torque perturbations.

This however makes for a complex device. Generally, solutions with flywheels have a couple of disadvantages, mainly to do with intrusiveness. The need for high rpm spinning masses, results in noticeable vibrations. Furthermore, the gyroscopic effect resists the change in orientation of the devices. The designs are also quite heavy and bulky.

The crank and cam mechanisms accelerate a mass asymmetrically with the help of an electric motor. The crank mechanism is able to produce the most repeatable 1DoF signal, while remaining relatively lightweight. However, it needs a second mass to counter the parasitic forces. Furthermore, there is little variability in the signal and a different mechanism is required to expand to multi-DoF

The devices that rely on periodic knocking as actuation principle generate a powerful (20N+) transient 1DoF pulses. The experimental data shows a very repeatable signal. However, these tests were performed statically. When used dynamically in daily life activities, the repeatability of the force is expected to be inadequate for system identification.

4.3 Table

In the table below, the state-of-the-art devices are sorted based on their actuation principle and perturbing mechanism. To judge its suitability for system identification, perturbation properties like maximum force/torque and signal shape are mentioned. General notes on intrusiveness are mentioned together with the force-to-weight ratio and the way the device is mounted to the limb. Finally, some relevant solution specific notes are mentioned.

	Actuation principle	Perturbing mechanism	Mounting solution	Load properties	Pure force/torque	Signal properties	Force-to-weight	Intrusiveness	Solution specific properties
Xu (1991)	Pneumatic	Airjet	Wrist mounted	Force: 4N 1DoF	No	Stochastic (random binary) 75Hz	Scalable	80-110dB noise	5.5 bar, smart valve based on Coanda principle
Gurocak (2003)				Force: 7.3N 3 DoF	No	Stochastic 15Hz	Scalable	6 pneumatic hoses running along arm	5.5 bar, force in arbitrary direction, servo valves
Belden (2011)				Force: 1.34 - 1.64E-4 N/Pa 1 DoF	No	Stochastic (random binary) 10Hz	0.075kg, scalable FTW 993.3	Noise	Design based on Xu (1991). Focussed on experimental validation
Höppner (2010)		Accelerating mass	Wrist mounted	Force: 1300N 1DoF	No	Transient 14ms	0.5kg, scalable FTW 2600	Length of cylinder ±130mm	5 bar
Hondori (2011)	Electromagnetic (Rotational)	Centrifugal force	Hand-held	Force: 7N 2 DoF	Yes	Sinusoidal 15Hz	Scalable	-	rotational mass 100g, at r = 2cm, n = 600rpm
Yano (2003), Murer (2015), Nakamura (2020), Antolini (2011)		Gyroscopic force	Hand-held	Torque: 118Nmm 3 DoF	No	Transient -	0.65kg, scalable TTW 182	High frequency vibrations	m = 100g, r = 2cm, n = 8000 rpm
Winfree (2009)				Torque: 1.2Nm 3 DoF	No	Transient -	0.49kg, scalable TTW 2449	Bulky	m = 138g, r = 4.5cm, n = <6600 rpm
Walker (2016), (Walker (2018))			Hand-held	Torque: 10-25Nmm (51.2Nmm) 3 DoF	Yes	Stochastic (binary) 1.25Hz, 200ms (150ms)	0.23kg, scalable TTW 43.5-109 (TTW 262)	High frequency vibrations, bulky	Torques generation in all arbitrary directions, torque cancelling
Choinière (2017), Amemiya (2013)		Asymmetric torque	Hand-held	Torque: 100Nmm 1 DoF	Yes	Stochastic (binary) 50Hz	0.33kg, scalable TTW 303	Gyroscopic effect, vibrations	Asymmetric torque by direct drive DC motor
Kakuda (2019)	Electromechanical	Cam mechanism	Hand-held	Force: 10-25N 1 DoF	No	Periodic 10Hz	-	Bulky	Results show bad repeatable force direction
Amemiya (2006)		Crank mechanism (Asymmetric oscillation)		Force: 17.5N (35N) 1 DoF	No (Yes)	Stochastic (binary) 10Hz	0.23kg, scalable (1.24kg) FTW 76.1	Bulky	Meant for wayfinding, directied for sensation (antiphase tandem pair)
Hamaguchi (2010)		Mass impact		Force: 24N 1 DoF	Yes	Periodic 5Hz	0.42kg, scalable FTW 57.1	Bulky	Force generation by continuous knocking by rotating mass
Shima (2012)				Force: 28.6N 1 DoF	Yes	Periodic 10Hz	0.23kg, scalable FTW 124	Long device	Force generation by impact of mass
Tanabe (2017)	Vibration speaker	Accelerating mass	Hand-held	Force: 1N 2 DoF	Yes	Periodic 75Hz	0.077kg, FTW 13	-	The transducer set-up enables both torques and forces
Culbertson (2016)	Voice coil			Force: 5N 1 DoF	Yes	Stochastic (binary) 100Hz	-	-	Possible to generate torques as well, this is however not mentioned
Sauvet (2017)	Piezoelectric			Force: 4.2N 1 DoF	Yes	Periodic 70Hz	0.26kg, scalable FTW 16.2	Bulky actuator, high voltage	Large range of forces with changing of mass

5 Discussion

A single gimballed flywheel setup can provide a 3DoF torque perturbation in arbitrary direction, while being relatively simple and compact. However, a perpendicular reaction torque with similar magnitude is also generated. This can be solved by a dual flywheel setup, resulting in a need for six motors. To get similar performance from the asymmetric torque principle, three flywheels and three motors are required.

In the presented scientific papers, high frequency (parasitic) vibrations have been mentioned when discussing fast spinning flywheels. Furthermore, flywheels induce gyroscopic stabilization, which result in unwanted resistance to movement in between perturbations. Winfree was able to solve this by allowing the flywheel to rotate freely in between pulses, however this required a much more complex control system.

The human limb is commonly modelled as a mass-spring-damper system. While performing system identification for such models, a force is most commonly used as input [18]. Torque inputs are possible to use, but require data fitting [11]. Forces also provide a more instinctive perturbation. They have a point of application and clear direction. The resulting displacement (acceleration) of the limb is also more straight-forward to measure with force perturbation.

The servos that position the flywheels have a limited range of motion, the bandwidth of pulses in the same direction is limited, since they require are certain washout period to return to their original position. A similar effect is present with the asymmetric torque solution. This is a reoccurring problem, also found outside the scope of rotating solutions. The mechanism/mass has to return from its stroke/rotation to apply another pulse in the same direction, resulting in the need for a returning force/torque. Only the pneumatic airjet principle does not suffer from this limitation and can offer a pure one-way pulse.

The pneumatic airjet principle is the superior actuator. It is easiest to scale up (with added pressure), with high achievable bandwidths, most versatile range of signals, and it is easily implemented with multiple DoF (while remaining lightweight). Furthermore, it has already been proven to work with system identification in the discussed literature. However, compared to electric solutions performs poorly when considering intrusiveness and freedom of movement. While other solutions require electric power from a power source like a battery, the power supply (pressure tank) and control electronics (valves) of pneumatic solutions are both heavy and big and need to be mounted externally. Resulting in multiple pneumatic hoses running up to the device, decreasing mobility. Discomforts during operation due to harsh sounds are more severe than those that electric solutions produce (vibrations). From this

can be concluded that pneumatic solutions in their current state-of-the-art form, are not suitable for ungrounded mechanical impedance measurements for day to day tasks.

Piezoelectric solutions are also considered unsuitable for our application. These actuators can generate an (unnecessarily) high force, while offering a very precise and small stroke. To get an useful stroke, a motion amplifier needs to be added. This results in a bulkier 1DoF setup than the other solutions. Furthermore, they generally require high voltage, which is deemed less safe when doing experiments with humans.

Some solutions rely on operating at the natural frequency to achieve a sufficient perturbation magnitude. As concluded by Sauvet, the system has to be tuned per test subject to get the required optimal performance. Since the resonance frequencies differ quite substantially in different postures and in different directions [25], these actuation principles are not as robust and repeatable as other solutions for our application.

Hondoris solution has a heavily frequency dependent perturbation force. With the centrifugal force as actuation principle one can not increase the perturbation frequency without changing the force as well. Furthermore, the proposed solutions introduces, in its current form, a low frequency periodic (repetitive) signal that will partly be suppressed by the central nervous system, and will therefore only be able to measure the reflexive stiffness.

Solutions that remain either combine electric actuators, both linear and rotating, with mechanisms like cams and cranks, or vibrational devices, like voicecoils/speakers. Voicecoil solutions provide easily controllable well determined low magnitude perturbations. The electromechanic solutions provide a higher force-to-weight ratio, but suffer from parasitic perturbation in undesired directions. Both remaining actuation principles are designed for a 1DoF perturbation, and only allow for multiple DoF pulses by simply adding the mechanism in more orthogonal directions. To get pure force perturbations in multiple DoF results in inefficient device (heavy/big) with one or more actuators and masses per DoF.

There is not a single actuation principle that can be directly implemented for our purpose. We are able to eliminate certain actuators due to unfavorable properties. An electric motor combined with a mechanism, has two non-critical flaws, mentioned above. To make this system work, a new mechanism has to be designed that suits the given requirements.

6 Conclusion

In this literature survey we set out to find the most suitable actuation principle for an ungrounded measurement device. The first step was to devise general criteria based on the application in which the actuator will be used. Next, the working principle and main properties of relevant state-of-the-art devices were analysed. These devices were then judged based on the given criteria.

Finally, we were able to eliminate certain actuation principles and converge to a suitable solution. Some quantitative values provided clear insights for comparison. However, since the actuation principle had to be implemented in an ungrounded device for use during day-to-day tasks, many (quantitatively) promising devices were not selected. Qualitative parameters turned out to be crucial in the selection process. While discussing the different actuation principles, the electromechanical (translational) options seem the most promising. They provide good force-to-weight ratios, with sufficient perturbation magnitudes (10-25N). Since this system is driven by low-speed electric motors, it suffers less from parasitic vibrations and gyroscopic effects. The solution can provide a very versatile range of perturbations due to scaling and tuning of the supporting mechanisms.

A challenging task lies ahead of selecting the right motor and mechanism combination. The new mechanism can be designed to be unintrusive and provide a range of input signals. By choosing an electromechanical system, we allow for the opportunity to design an efficient mutli-DoF pure force perturbator.

Bibliography

[1] Asmarani Ahmad Puzi, Naim Sidek, and Fatai Sado. Mechanical Impedance Modeling of Human Arm: A survey. *IOP Conference Series: Materials Science and Engineering* [online]. 184 (Mar. 2017), p. 012041. DOI: 10.1088/1757-899X/184/1/012041.

[2] Tomohiro Amemiya, Hideyuki Ando, and Taro Maeda. Directed force perception when holding a nongrounding force display in the air (Dec. 2006). DOI: 10.18974/tvrsj.11.4_545.

[3] Tomohiro Amemiya and Hiroaki Gomi. Directional Torque Perception with Brief, Asymmetric Net Rotation of a Flywheel. *IEEE Transactions on Haptics* [online]. 6 (July 2013), pp. 370–375. DOI: 10.1109/TOH.2012.38.

[4] Tomohiro Amemiya et al. "Double-layer slider-crank mechanism to generate pulling or pushing sensation without an external ground". In: Dec. 2007, pp. 2101–2106. DOI: 10.1109/IROS.2007.4399211.

[5] Tomohiro Amemiya et al. Double-layer slider-crank mechanism to generate pulling or pushing sensation without an external ground (2007), pp. 2101–2106. DOI: 10.1109/IROS.2007.4399211.

[6] Seonghoon Ban and Kyung Hoon Hyun. Directional Force Feedback: Mechanical Force Concentration for Immersive Experience in Virtual Reality. *Applied Sciences* [online]. 9 (Sept. 2019), p. 3692. DOI: 10.3390/app9183692.

[7] Jesse Belden et al. A portable air jet actuator device for mechanical system identification. *The Review of scientific instruments* [online]. 82 (Mar. 2011), p. 035106. DOI: 10.1063/1.3562894.

[8] Amy Blank, Allison Okamura, and Louis Whitcomb. "Task-dependent impedance improves user performance with a virtual prosthetic arm". In: May 2011, pp. 2235–2242. DOI: 10.1109/ICRA.2011.5980461.

[9] Jean-Philippe Choiniere and Clément Gosselin. Development and Experimental Validation of a Haptic Compass Based on Asymmetric Torque Stimuli. *IEEE Transactions on Haptics* [online]. 10 (June 2016), pp. 1–1. DOI: 10.1109/TOH.2016.2580144.

[10] Heather Culbertson, Julie Walker, and Allison Okamura. "Modeling and Design of Asymmetric Vibrations to Induce Ungrounded Pulling Sensation Through Asymmetric Skin Displacement". In: Apr. 2016. DOI: 10.1109/HAPTICS.2016.7463151.

[11] Diego Guarin and Robert Kearney. Unbiased Estimation of Human Joint Intrinsic Mechanical Properties During Movement. *IEEE Transactions on Neural Systems and Rehabilitation Engineering* [online]. PP (Sept. 2018), p. 1. DOI: 10.1109/TNSRE.2018.2870330.

[12] Hakan Gurocak et al. Weight Sensation in Virtual Environments Using a Haptic Device With Air Jets. *J. Comput. Inf. Sci. Eng.* [online]. 3 (June 2003), pp. 130–135. DOI: 10.1115/1.1576808.

[13] Hidenori Hamaguchi et al. "Design of repetitive knocking force display for being-pulled illusion". In: Oct. 2010, pp. 33–37. DOI: 10.1109/ROMAN.2010.5598717.

[14] Frans C. T. van der Helm Herman van der Kooij Bart Koopman. Human Motion Control (Jan. 2003).

[15] Hannes Höppner et al. "The Arm-Perturbator: Design of a Wearable Perturbation Device to measure Limb Impedance". In: Oct. 2010.

[16] Zhao-Hui Jiang. Impedance Control of Flexible Robot Arms with Parametric Uncertainties. *Journal of Intelligent and Robotic Systems* [online]. 42 (Feb. 2005), pp. 113–133. DOI: 10.1007/s10846-005-0933-x.

[17] Emi Kakuda et al. "Study on sub-Optimal Rotation Speed and Cam Shape for Ungrounded Force Display using Grooved Cam". In: Oct. 2019, pp. 6952–6956. DOI: 10.1109/IECON.2019.8927478.

[18] Robert Kearney and Ian Hunter. System Identification of Human Joint Dynamics. *Critical reviews in biomedical engineering*. 18 (Feb. 1990), pp. 55–87.

[19] Takehito Kikuchi et al. Quasi-3-DOF Rehabilitation System for Upper Limbs: Its Force-Feedback Mechanism and Software for Rehabilitation (July 2007), pp. 24–27. DOI: 10.1109/ICORR.2007.4428401.

[20] Editha Loon et al. Changes in Limb Stiffness Under Conditions of Mental Stress. *Journal of motor behavior* [online]. 33 (July 2001), pp. 153–64. DOI: 10.1080/00222890109603147.

[21] Hossein Mousavi Hondori and Ling Shih-Fu. Perturbation-based Measurement of Real and Imaginary Parts of Human Arm's Mechanical Impedance. *Conference proceedings : ... Annual International Conference of the IEEE Engineering in Medicine and Biology Society. IEEE Engineering in Medicine and Biology Society. Conference* [online]. 2010 (Aug. 2010), pp. 5911–4. DOI: 10.1109/IEMBS.2010.5627544.

[22] Hossein Mousavi Hondori and Ang Tech. Smart mug to measure hand's geometrical mechanical impedance. *Conference proceedings : ... Annual International Conference of the IEEE Engineering in Medicine and Biology Society. IEEE Engineering in Medicine and Biology Society. Conference* [online]. 2011 (Aug. 2011), pp. 4053–6. DOI: 10.1109/IEMBS.2011.6091007.

[23] Winfred Mugge et al. Sensory Weighting of Force and Position Feedback in Human Motor Control Tasks. *The Journal of neuroscience : the official journal of the Society for Neuroscience* [online]. 29 (May 2009), pp. 5476–82. DOI: 10.1523/JNEUROSCI.0116-09.2009.

[24] Yves Rybarczyk et al. The development of robot human-like behaviour for an efficient human-machine co-operation (Jan. 2001).

[25] Bruno Sauvet, T. Laliberté, and Clément Gosselin. Design, analysis and experimental validation of an ungrounded haptic interface using a piezoelectric actuator. *Mechatronics* [online]. 45 (Aug. 2017), pp. 100–109. DOI: 10.1016/j.mechatronics.2017.06.006.

[26] Takuya Shima and Kenjiro Takemura. "An Ungrounded Pulling Force Feedback Device Using Periodical Vibration-Impact". In: vol. 7282. June 2012, pp. 481–492. ISBN: 978-3-642-31400-1. DOI: 10.1007/978-3-642-31401-8_43.

[27] Takeshi Tanabe, Hiroaki Yano, and Hiroo Iwata. "Temporal characteristics of non-grounded translational force and torque display using asymmetric vibrations". In: June 2017, pp. 310–315. DOI: 10.1109/WHC.2017.7989920.

[28] Julie Walker et al. "A Dual-Flywheel Ungrounded Haptic Feedback System Provides Single-Axis Moment Pulses for Clear Direction Signals". In: Apr. 2016. DOI: 10.1109/HAPTICS.2016.7463148.

[29] Julie Walker et al. "A Dual-Flywheel Ungrounded Haptic Feedback System Provides Single-Axis Moment Pulses for Clear Direction Signals". In: Apr. 2016. DOI: 10.1109/HAPTICS.2016.7463148.

[30] Julie Walker et al. Haptic Orientation Guidance Using Two Parallel Double-Gimbal Control Moment Gyroscopes. *IEEE Transactions on Haptics* [online]. PP (June 2017), pp. 1–1. DOI: 10.1109/TOH.2017.2713380.

[31] Kyle Winfree et al. A High Fidelity Ungrounded Torque Feedback Device: The iTorqU 2.0. *Departmental Papers (ESE)* [online] (Apr. 2009). DOI: 10.1109/WHC.2009.4810866.

[32] Hiroaki Yano, M. Yoshie, and Hiroo Iwata. "Development of a non-grounded haptic interface using the gyro effect". In: Apr. 2003, pp. 32–39. ISBN: 0-7695-1890-7. DOI: 10.1109/HAPTIC.2003.1191223.

[33] Chien-Hsien Yeh et al. Application of Piezoelectric Actuator to Simplified Haptic Feedback System. *Sensors and Actuators A: Physical* [online]. 303 (Mar. 2020), p. 111820. DOI: 10.1016/j.sna.2019.111820.

[34] Xu YMj et al. An Airjet Actuator System for Identification of the Human Arm Joint Mechanical Properties. *IEEE transactions on bio-medical engineering* [online]. 38 (Dec. 1991), pp. 1111–22. DOI: 10.1109/10.99075.

Scientific Paper

Design and validation of ungrounded wrist perturbator based on parallel mechanism.

Robbert Koene

4497902

MSc High-Tech Engineering

Delft University of Technology

Design and Validation of Ungrounded Wrist Perturbator Based On Parallel Mechanism

Robbert Koene, *Student,* Volkert van der Wijk, *Assistant Professor*

***Abstract*—The compliance (stiffness) of a human arm varies, depending on the task at hand. Some precise tasks require high stiffness, while others need a level of flexibility to deal with unknown disturbances. To describe this human behaviour a portable device is needed to give small force perturbations (input) while the resulting reaction of the arm (output) is measured. There are multiple state-of-the-art devices to choose from to provide such input. However, the majority of these devices either offer too little versatility or impede the free movement of the user. Implementation of a novel parallel mechanism allows for a lightweight (0.175kg) and compact device that can generate various signals in three degrees-of-freedom. Since the device is designed to be mounted around the wrist, it leaves your arm and hand unobstructed. A full-scale prototype is constructed and the concept is tested using a force sensor. Implementing powerful yet compact servo motors allows for controlled perturbations in the order of 4N, with bandwidths up to 12Hz.**

***Index Terms*—Force perturbation, human arm, system identification, robotics, parallel mechanism, mechatronics**

I. Introduction

SYSTEM identification has been used for decades to determine the mechanical properties of the human limbs [1]. Originally, these experiments were performed in the lab by means of position perturbations. Due to scientific developments in the field of robotics [2] and healthcare [3], measurements need to be taken out of the intrusive lab environment. By making the measurement device wearable and changing to a force perturbation, it is possible to do experiments during daily tasks without impeding voluntary movement.

Limiting ourselves to arm pertubators, state-of-the-art research has provided a multitude of portable devices, differing mainly in actuation principle and the resulting specifications. Using pneumatics, it is possible to generate well-defined and versatile perturbation signals. By implementing the airjet principle [4] a force of 4N and frequency of 75Hz is achievable. A three degree-of-freedom (DoF) solution [5] is realised by attaching a block with multiple outlets on your wrist. The working principle behind these designs is the venting of pressurized air to the atmosphere, generating considerable noise. Using the air pressure to move a mass [6], in stead of venting it into the atmosphere, results in a quieter device. Still, the major drawback for all these systems however lies with the bulky peripheral equipment (e.g. pressure tank, hoses, valves) needed.

Electro-mechanical solutions exist in the form of rotating and translating assemblies. Rotating assemblies can generate ungrounded force or torque perturbations by using flywheel inertia [7] or the gyroscopic effect [8]. However, the gyroscopic stabilization of rotating bodies impedes voluntary movement. Current translational solutions consist of crank [9] and cam [10] mechanisms, able to produce high amplitude and repeatable force perturbations. Unfortunately, these 1DoF mechanisms generate substantial parasitic forces.

The majority of the current electro-mechanical solutions are designed to be used on the arm. Still, little effort is made to integrate these devices for unimpeded use. Some devices are placed on the wrist off-axially, resulting in torques being induced next to the desired perturbing force. The other solutions are big rectangular or cylindrical objects and therefore are forced to be hand-held. Moreover, most existing actuation principles offer 1DoF impulses. Expanding to multi-DoF perturbations is possible by adding the system to each principal direction. However, this would result in inefficient and bulky devices.

The goal of this paper is to present a proof-of-concept mechatronic system that is designed to generate controlled force perturbations in three degrees-of-freedom. This is achieved by using high performance electric motors together with a novel orientation of a parallel mechanism. Being meant as a tool for non-intrusive system identification, holistic design decisions are made with this in mind. First, the chosen mechanism and its kinematics will be explained. Then, the prototype will be presented with its main dimensional specifications and the chosen actuator. Finally, the performance of the prototype will be validated experimentally and future points for improvement discussed.

II. Conceptual Design

The working principle behind the design is based on Newton's second and third law of motion, where the acceleration (and/or deceleration) of a mass results in a reaction force proportional and opposite to this acceleration. This relation enables a lightweight design to generate a suitably large perturbation, as long as the mechanism can provide ample acceleration.

A. Mechanism

To generate perturbing forces along the three principal axes (XYZ), one must allow for three translational degrees-of-freedom. Implementing a parallel mechanism is an efficient way to constrain unwanted motion in the other directions. Parallel mechanisms offer a high stiffness and are known for their good dynamic behaviour [11]. For this particular application the Delta mechanism [12] offered a suitable starting point.

In order to get perturbation forces to act through the central axis of the arm, the mechanism must be constructed around

the wrist. By doing this, a useful perturbation signal can be generated while keeping your hands free for daily tasks. Therefore, the base of the mechanism was chosen to be a ring, tightly fitted around the wrist, as can be seen in Figure 1. The moving part of the mechanism, in robotics called the end-effector, is a ring with a larger diameter than the base, to accommodate 3-DoF displacement. In industry it is unusual for the end-effector (outer ring) to be heavy and big, since this inhibits high speed and precise movement. However, this anti-balance is exactly what is needed for this application to induce maximum reaction forces.

Reconsidering the orientation of the Delta mechanism was necessary to have the end-effector move in the same plane as the base. This resulted in a new mechanism, as shown in Figure 2), which not only allowed for a more compact device, but also a force perturbation that does not inherently also induces a reaction torques.

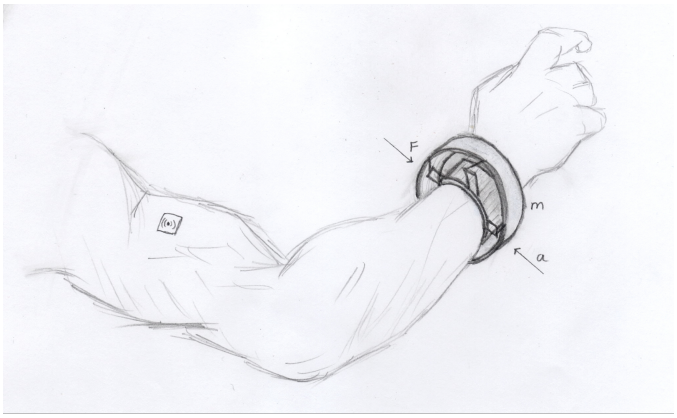

Fig. 1. Concept sketch of device with re-imagined parallel mechanism, plus inner and outer ring. Enabling free movement while doing measurements.

B. Kinematics

The perturbing force is directly related to the acceleration signal. This signal dictates the position of the outer ring (mass) over time. Using inverse kinematics, the required motion of the motors is calculated back from the outer ring trajectory.

A single chain of the mechanism consists of a 1DoF rotational joint (servo motor) connected to four 2DoF universal joints, arranged such that they form a four-bar linkage (lower arms). Two methods were used to describe the inverse kinematics, each with their own purpose. The first method [13] results in a differentiable function, that was used to do stability analysis.

The second method [14] uses the allowed movement of the upper and lower arm to find at which position the joints intersect. This method is computationally less demanding. The desired outer ring trajectory is discretized into steps at a multiple of the control frequency. A MATLAB script performs the necessary operations to output the discrete motor (angle) positions.

C. Singularities, stiffness, and redundancy

The reorientation of the parallel mechanism caused undesired singularities, resulting in the addition of a fourth redundant member. When moving through the mechanisms' workspace, singularities present themselves as positions where it is possible to move the end-effector without moving the motors. Play in the joints of the mechanism increased the sensitivity of the mechanism to end up in these singularities.

A property of parallel mechanisms is that adding members results in averaging of the play and an increase of stiffness [11]. In the case of the Delta-like mechanisms, a fully-constrained system consists of three arms. To overcome the singularities a fourth arm is added, making the mechanism over-constrained. At the risk of generating critical internal forces in the mechanism, the addition of redundant members has often been proven to result in a performance increase [15].

The sensitivity to singularities and the condition number as a result of the arm lengths were also examined. It could be concluded that the angle that both upper and lower arm span with the XY-plane, must be close to 45 degrees. The resulting arm lengths are then dependent on the diameter of inner and outer ring.

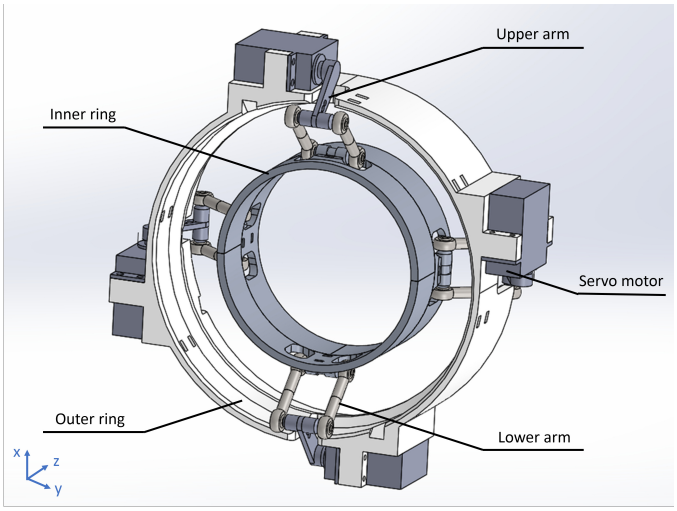

Fig. 2. CAD model of thee prototype, with the main parts highlighted.

III. Prototype

A. Prototype with final dimensions

The final CAD design can be seen in Figure 2. Unconventional for a parallel robot is the position of the motors, mounted on the end-effector. This was done to increase the moving mass, while keeping the total weight of the device low. The two pairs of arms are offset in Z-directions to allow for a stiffer outer ring. All relevant dimensions and weights, that are also labeled in Figure 2, are presented in Table I.

To speed up the prototyping, mostly off-the-shelf components were selected. This resulted in micro ball joints being used in stead of universal joints, making the lower arms under-constrained. This however does not negatively affect the functioning of the redundant parallel mechanism. Both inner and outer ring were manufactured using 3D printing, the final result of which can be seen in Figure 3. In this version, you are also able to split the inner ring, making it possible to mount it to the wrist/experimental setup. The design could

benefit from a stiffer material than PLA plastic. However, 3D printing enabled us to do quick iterations and keep the cost down.

TABLE I
RELEVANT DESIGN PARAMETERS

Outer ring diameter	128mm
Inner ring diameter	71.44mm
Upper arm length	19mm
Lower arm length	22.5mm
Z-offset arms	11.4mm
Moving mass	0.146kg
Total mass	0.175kg

B. Actuation

For this prototype the KST DS215MG V3.0 servo motor was selected as the method of actuation. Next to the performance, their ease of use aids the possibility to perform quick prototyping. In one package, the servo offers a gearbox, encoder, and internal controller. There is no need for additional motor drives and the positional control is simple. Furthermore, they are strong and robust and due to two ball bearings the motor acts as a stiff 1DoF rotational joint.

Even with a small footprint and low weight, the servo offers a high torque at relatively high rated speeds (see Table I). The motor operates at 7.4 volts, which is the rated voltage of compact two cell LiPo battery packs. Also, this operating voltage is safe to use for human interaction.

TABLE II
KST DS215MG V3.0 SERVO MOTOR SPECIFICATIONS

Operating voltage	6.0V	7.4V
Torque [Nm]	0.30	0.36
Angular velocity [rad/s]	34.9	41.9
Control frequency	333Hz	
Dimensions (l*w*h)	23*12*27.5mm	
Weight	20g	

The internal feedback loop does result in a rather unconventional control method. Where the input signal is a position (angle) rather than a torque/current. No position data from the encoder is sent back, nor are the control parameters tuneable. The angular inputs are given by an Arduino Nano, communicating via a pulse width modulated (PWM) signal.

C. Trajectory planning

The parallel mechanism enables the outer ring to move along the three principle axes (XYZ) as well as the combinations of these axes (e.g. in the XZ-plane). The trajectory can be programmed in such a way that the outer ring generates either a transient or periodic pulse. The signal shape is determined by the acceleration profile of the moving mass. Since the application of this device is system identification, a block wave signal seemed fitting.

The MATLAB algorithm, with at its core the inverse kinematics, has two inputs: displacement (e.g. x -0.005 to 0.005m) and an acceleration (multiplied by mass equals perturbing force). Dependent variables, like the pulse length and number of data points are then calculated. The algorithm then outputs an array with motor angles, which is then converted with a calibrated value for each motor.

These angles can be used as an input for the Simscape Multibody model, which was used to simulate the dynamics of the device. The model has the same dimensions and weights as the real world prototype. When ran, it outputs useful parameters such as the reaction forces and torques on the base (wrist). Furthermore, it plots the torque and velocity needed for each servo to accomplish the trajectory. The data from the simulation can be used to predict behaviour for the respective trajectories.

IV. EXPERIMENTAL MEASUREMENTS

A. Experimental setup

The sensor that was used to validate the design is the ATI mini45. This is a 6DoF sensor that measures both reaction forces and reaction torques. The output data is sampled at 10kHz, passed through a 5V amplifier and then processed by a NI USB-6361 DAQ. Via a USB-connection the six voltage channels are fed into a MATLAB script. Here, they are multiplied with a calibration matrix that converts them into force and torque values. Each measurement begins with the prototype powered on and in its neutral position. The first few data points of each measurement are then averaged and subtracted from the signal, to correct for the zero offset and gravity.

To mount the prototype to the 6DoF sensor an adapter was designed and 3D printed. The setup can be seen in Figure 3. For the prototype's intended use, the wrist would be in the position of the this adapter. Because the adapter creates an offset between the force's point of engagement and the sensor, some reaction torques are generated which would not be there when mounted on the wrist. This must be corrected for in the torque data.

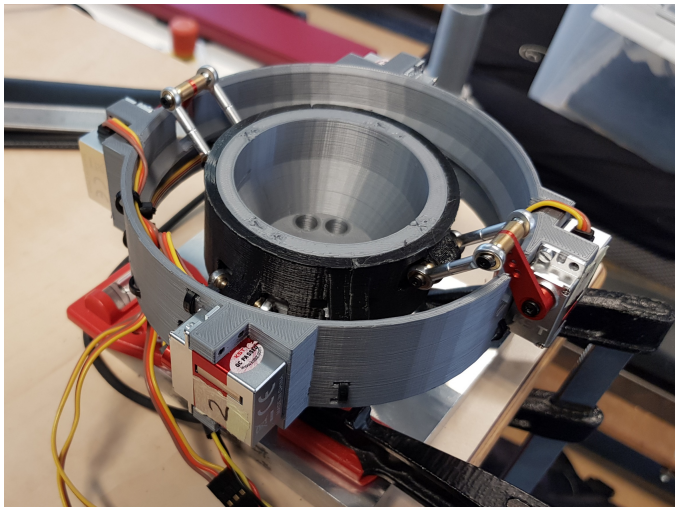

Fig. 3. The perturbator prototype mounted on the 6DoF force sensor

B. Experiments

As a preparation for the final performance experiment, some initial tests were performed to check the control method

and overall functioning of the system. From here, it was empirically determined that the motors maximum rotational velocity was 32 rad/s, when under load. This parameter was fed back into MATLAB and simulink for future path planning.

Only during the first experiments it became clear that this rotational velocity was severely limiting the capabilities of the device. At larger displacements and high accelerations, the motors quickly reached their top speed during the trajectory. High perturbing forces (8N) were still achievable, however this required another force signal (no block wave) or increasing the weight of the outer ring. Choosing a block wave with the current design therefore does not give the highest possible force, but it is one of the more useful signals to describe the behaviour of the system.

The following tests were performed: a 3N periodic and 4N transient pulse in X,Y, and Z-direction. Since the device will be used during daily tasks, the gravitational acceleration will not always point in the same direction. Therefore, the device is tested both horizontally (as in Figure 3) and vertically (90°rotated). In the figures, the average force is displayed with a solid line and the standard deviation is represented by the dotted line.

C. Results

The results of the periodic tests are shown in Figure 4 below, together with the theoretical force signal. There are a few things that need to be mentioned when looking at these results. While a periodic signal can be detected, it does not entirely resemble the desired block wave. The plots represent one full cycle of the mechanism. The zero-crossing occurs halfway through the trajectory, when the outer mass goes from being accelerated to being decelerated. A quarter period to both sides from here, a dip occurs. This is most likely due to the motors having to switch directions here. The other dips in the signal were accounted to the internal controller of the servos. Processing angular inputs at 333Hz (every 3ms), was deemed to slow for this application. To prove this theory, the (moving) mass was increased while keeping the desired force the same, which resulted in more data points and a smoother signal. Finally, it can be observed that the signal does seem to be consistent, independent of the orientation of the device.

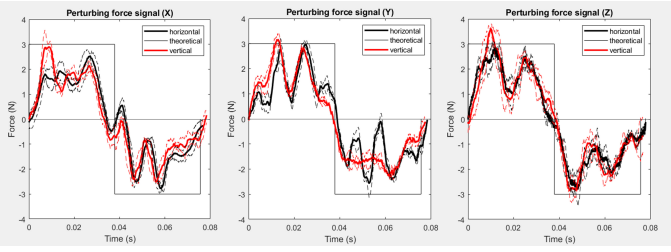

Fig. 4. 3N pulse in XYZ-direction (black), with setup rotated 90 °around Y-axis (red), n=4

Figure 5 shows the transient signals of a one-way trajectory the in XYZ-directions. While the magnitude of 4N is reached during deceleration, this is a peak value. The signal is smoother during acceleration, but does not reach the target magnitude. This could be a result of backlash in the joints, or the unfavorable position of the arms at the edges of the workspace. Combine this with the non-optimal controller and this can result in under/overshoot.

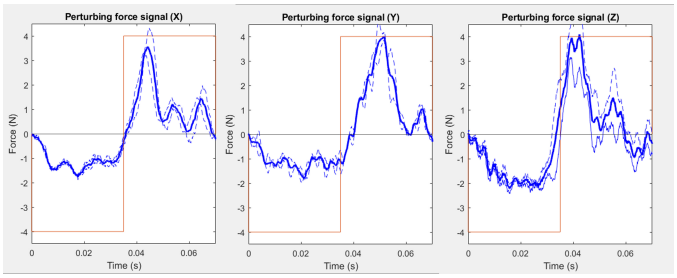

Fig. 5. 4N transient pulse in XYZ direction, n=3

In the previously shown figures, only the forces in the desired perturbing direction were display for clarity. However, unwanted reaction forces and torques in other directions also occur, mainly during movement in X or Y direction. Their magnitude compared to the main signal is shown in Figure 6. Note that the sensor always outputs noise with a magnitude of around 0.2N. Only the reaction force in Z-directions deviates significantly from the theoretical values simulated by the Simulink model. This behaviour is expected to be a result of the lack of stiffness at the extreme positions in the trajectory. Since during the experiments, it could be observed that the outer ring slighty dips/tilts here.

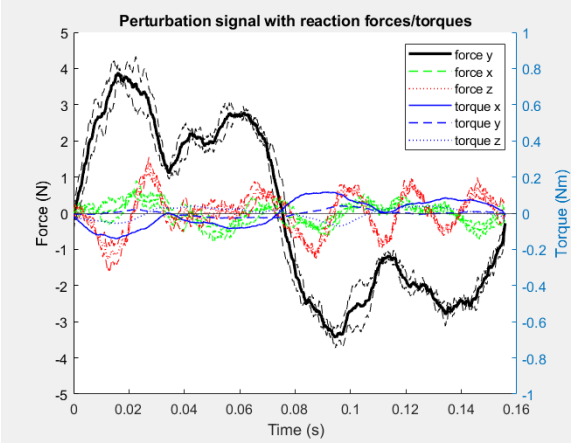

Fig. 6. A 4N signal in Y-direction (black line), with parasitic reaction forces and torques.

D. Interpreted specifications

The signal that can be generated by the perturbing device is a trade-off between different parameters. The force magnitude is determined by the weight of the moving mass and the acceleration. In turn, the acceleration together with the size of the stroke influence the pulse length and maximum bandwidth. The shape and size of the perturbation is therefore up to the user, and not all combinations have been evaluated.

However, some broad specifications can be derived from interpreting the physical model and the experimental data.

The maximum travel was measured to be 16mm. The nominal force for square wave signals is limited to roughly 4N, at a maximum bandwidth of 12Hz. These signals are repeatable with an average standard deviation of 0.20N, 0.22N, and 0.53N in XYZ-direction respectively. A maximum force of around 8N for high frequency peak pulses was measured.

V. Discussion

The fourth redundant arm increased the mechanisms stiffness, while decreasing its sensitivity to end up in singular positions. However, near the limits of the workspace in Z-directions, singular positions still exist. Generally, the stiffness decreases when moving away from neutral position. Additional sensitivity is the result of significant play in the ball joints. Some hysteresis is observable in the results from the periodic experiments. Improving the build quality of the mechanism will solve a lot of these issues. It is recommended to produce precise universal joints, design stiffer rings, and optimize the geometry parameters to the desired perturbing signal.

As for the actuation and control, it became clear that the actuator selection should be reconsidered. While the servo motor offered an easy starting point for prototyping, the lack of control authority resulted in poor set point tracking. Especially with a redundant mechanism, which benefits from customized control [16]. Finally, the motors gear ratio can be optimized (reduce ratio), to increase the maximum angular velocity and make better use of the available travel.

The wrist perturbator as a concept, based on a parallel mechanism and electric motors, shows promising results. To implement it for human research, a few steps have to be taken. First, a suitable sensor setup must be conceived to measure the response of the arm to the known force perturbation. Also, the interface between the perturbator and the arm needs to be studied for optimal force transmission (stiffness). The current design already allows for moulded adapters to be placed within the inner ring to provide a tight fit with the wrist.

In its current form, the perturbator does not offer a direct contribution to the field of robotics. It could however serve as a high performance parallel manipulator when the inner ring is again used as end-effector. The main attribute would be the ability to do pick-and-place manipulation in an application with little available space. Furthermore, this setup could serve as a positioning stage, as part of a larger machine or robot.

VI. Conclusion

In this paper, a proof-of-concept mechatronic system was presented that is able to generate ungrounded force perturbations for measurements on the human arm. The biggest advantages of the perturbator, compared to the state-of-the-art, is its versatility. It can offer a 4N transient or periodic (12Hz) force signal in three degrees-of-freedom, with high repeatability. Furthermore, because it was designed to be wrist mounted and lightweight (0.175kg), there is minimal hindrance of movement during experiments.

A novel implementation of a parallel mechanism was worked out to fit in a small package and minimize parasitic torques. Powerful servo motors were selected to redundantly actuate the mechanism. From here, a prototype was constructed and its performance experimentally determined. The results confirmed the viability of the concept. The performance could still be improved further with dedicated motor control.

References

[1] R. Kearney and I. Hunter, "System identification of human joint dynamics," *Critical reviews in biomedical engineering*, vol. 18, pp. 55–87, 02 1990.

[2] F. Angelini, C. Della Santina, M. Garabini, M. Bianchi, and A. Bicchi, "Control architecture for human-like motion with applications to articulated soft robots," *Frontiers in Robotics and AI*, vol. 7, 2020. [Online]. Available: https://www.frontiersin.org/article/10.3389/frobt.2020.00117

[3] L. Piggott, S. Wagner, and M. Ziat, "Haptic neurorehabilitation and virtual reality for upper limb paralysis: A review," *Critical Reviews in Biomedical Engineering*, vol. 44, 01 2016.

[4] Y. Xu, I. W. Hunter, J. M. Hollerbach, and D. J. Bennett, "An airjet actuator system for identification of the human arm joint mechanical properties," *IEEE Transactions on Biomedical Engineering*, vol. 38, pp. 1111–1122, 1991.

[5] H. Gurocak, S. Jayaram, B. Parrish, and U. Jayaram, "Weight sensation in virtual environments using a haptic device with air jets," *J. Comput. Inf. Sci. Eng.*, vol. 3, pp. 130–135, 06 2003.

[6] H. Höppner, D. Lakatos, H. Urbanek, and P. van der Smagt, "The arm-perturbator: Design of a wearable perturbation device to measure limb impedance," 10 2010.

[7] J. M. Walker, M. Raitor, A. Mallery, H. Culbertson, P. Stolka, and A. M. Okamura, "A dual-flywheel ungrounded haptic feedback system provides single-axis moment pulses for clear direction signals," in *2016 IEEE Haptics Symposium (HAPTICS)*, 2016, pp. 7–13.

[8] H. Mousavi Hondori and A. Tech, "Smart mug to measure hand's geometrical mechanical impedance," *Conference proceedings : ... Annual International Conference of the IEEE Engineering in Medicine and Biology Society. IEEE Engineering in Medicine and Biology Society. Conference*, vol. 2011, pp. 4053–6, 08 2011.

[9] T. Amemiya, I. Kawabuchi, H. Ando, and T. Maeda, "Double-layer slider-crank mechanism to generate pulling or pushing sensation without an external ground," in *2007 IEEE/RSJ International Conference on Intelligent Robots and Systems*, 2007, pp. 2101–2106.

[10] E. Kakuda, S. Yokota, A. Matsumoto, D. Chugo, and H. Hashimoto, "Concept verification of ungrounded force display using cam," in *2018 11th International Conference on Human System Interaction (HSI)*, 2018, pp. 432–437.

[11] Y. Patel and P. George, "Parallel manipulators applications—a survey," *Modern Mechanical Engineering*, vol. 2, pp. 57–64, 08 2012.

[12] R. Clavel, "Conception d'un robot parallèle rapide à 4 degrés de liberté," 1991.

[13] R. L. Williams II, "The delta parallel robot: Kinematics solutions," *Mechanical Engineering, Ohio University*, 10 2016.

[14] H. Elias, "Inverse kinematics of parallel manipulator (delta robot)," Oct 2014. [Online]. Available: https://robotics.stackexchange.com/questions/3144/inverse-kinematics-of-parallel-manipulator-delta-robot

[15] D. Corbel, M. Gouttefarde, O. Company, and F. Pierrot, "Towards 100g with pkm. is actuation redundancy a good solution for pick-and-place?" pp. 4675–4682, 2010.

[16] S. Nokleby, R. Fisher, R. Podhorodeski, and F. Firmani, "Force capabilities of redundantly-actuated parallel manipulators," *Mechanism and Machine Theory*, vol. 40, no. 5, pp. 578–599, 2005.

4 Discussion

In the literature survey, ungrounded perturbing devices from multiple different research fields were discussed. The goal was to find the most promising actuator method for our specific application. Based on criteria that were set up for this application, an electromechanical actuator was deemed most promising. Existing devices showed great promise in terms of quantitative properties, like force-to-weight ratio and repeatability. The combination of an electric motor and a yet to design mechanism also offered the freedom to design an non-intrusive device to generate the required perturbations.

Looking back, it can now be determined whether this decision was justified. When adding the paper that was written to the state-of-the-art literature from the literature survey, some relevant parameters and properties can be compared. In its current form, the wearable perturbator can generate repeatable signals with a magnitude of around 4N. Devices from literature were able to produce 20+ N impulses. When comparing the force-to-weight ratio, some state-of-the-art devices perform better. However, in the discussed literature there were only two devices that could efficiently produce transient and periodic 3DoF perturbations, the pneumatic device from Gurocak and the flywheel design from Walker. Compared to these devices, the new perturbator offered the same functionality, but in a much less intrusive manner. Movement is unhindered and the hand is kept free to perform daily tasks. In short, by limiting ourselves to a translational electromechanical solution, as was suggested from the literature survey, it was possible to implement a mechanism into a holistic design to generate versatile perturbations. Therefore, this choice is still deemed valid.

While the proof-of-concept design was created for the application of system identification in the field of biomechanical engineering, it could be relevant in other fields of research as well. Multiple state-of-the-art devices that were found during the literature survey were intended for haptic wayfinding. The signal that was used during the experiments would not have been useful, since it consisted of a pulse in one direction and a similar recovering pulse in the opposite direction. To get a single directional pulse, the trajectory could easily be programmed to stretch this recovery period and make it unnoticeable. As for robotics, when considering the field of manipulators, the current setup is not ideal. The extra mass in the form of a pay-load is added to an already heavy end-effector. Powerful actuators are necessary to achieve acceptable accelerations and the large unbalanced moving mass results in vibrations and imprecise positioning. However, using the inner ring as end-effector results in a device with some desirable specifications. Now the moving mass is low, and while moving in plane, little reaction forces and torques are generated. If a situation calls for fast, small-stroke and (close to) in-plane manipulation, the parallel mechanism designed for the perturbator prototype offers a great solution. Furthermore, in its current form, the device would be well suited as a positioning device.

For example, when a large serial robot is used to manipulate something on a big reach. The compact parallel mechanism could be placed on the final stage to stabilize movement and help with disturbance rejection.

5 Conclusion

In this master's thesis a new mechatronic device was designed to provide an input for system identification on the human arm. A literature survey was conducted, which offered a framework of criteria and actuation principles. State-of-the-art devices were not directly suitable. Therefore, it was advised to combine a mechanism with electric actuators for the thesis research. This research resulted in a proof-of-concept prototype with favourable properties. At 175 grams, the device is lightweight and is designed to be mounted on the wrist, leaving your hands free to perform tasks. A novel implementation of an existing parallel mechanism together with powerful electric motors enabled the device to generate versatile 3DoF ungrounded perturbations. Both transient and periodic pulses can be repeatably generated up to a magnitude of 4N and a bandwidth of 12Hz. The concept is promising and can be improved further by implementing a bespoke controller.

The main contribution is considered to be the redundant 3DoF mechanism developed for this application. With design decisions focused on generating the most useful signals. It is also small in size, lightweight, and generates minimal parasitic forces and torques while moving in-plane. Taken outside the scope of this research, it might also be relevant in the field of robotics for manipulation or positioning.

6 Appendix

This chapter of the report focuses in more depth on some design steps and details that were not covered in the paper.

6.1 Kinematics and stability

6.1.1 Vector notation kinematics

The first method to determine the inverse kinematic relation is based on vector notation. In Figure 6.1 a schematic image is shown that resembles one arm of the mechanism. Where PB is center position in XYZ of the outer ring. B1 is the distance from PB to the joint on the outer ring (the radius). L1 represents the upper arm, l1 the lower arm. P1 is the distance from the origin to the joint on the inner ring. By vector addition, these variables result in the shown equation.

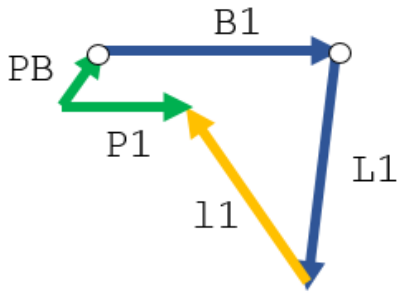


```
P1 - PB = B1 + L1 + l1;
l1 = P1 - PB - B1 - L1;
```

Figure 6.1: Vector representation of system

Next, with this notation established, vectors can be assigned to the variables. Certain parameters need to be specified, like the diameter of the inner and outer ring, arm lengths and the XYZ-position of the outer ring (end-effector). Plugging these values in the equation from Figure 6.1, results in the (inverse) kinematic relation. The relations are now dependent on the variable theta, which represents the angles of the motors. Theta is zero when the upper arm is parallel with the xy-plane. Solving the

set of equations results in two possible angles per motor. With this information an illustrative plot can be made as shown in Figure 6.2.

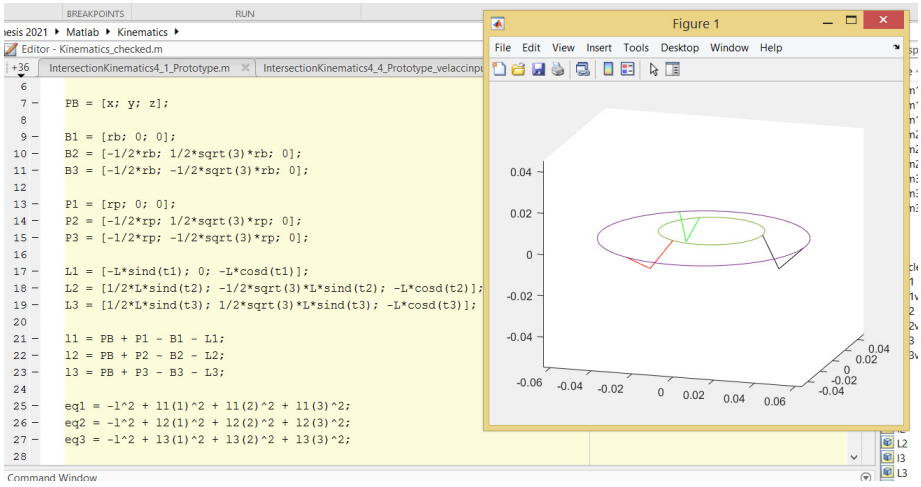

Figure 6.2: Visual representation using kinematic equation

With the kinematic equations sorted, it is possible to simulate a simple trajectory and gain knowledge on the movement of the motors. For example a sweep in x-direction from -0.005mm to 0.005mm. Figure 6.3 represents the required rotation of the individual motors as a function of the position in x. (Note that for this example, the old non-redundant mechanism was used).

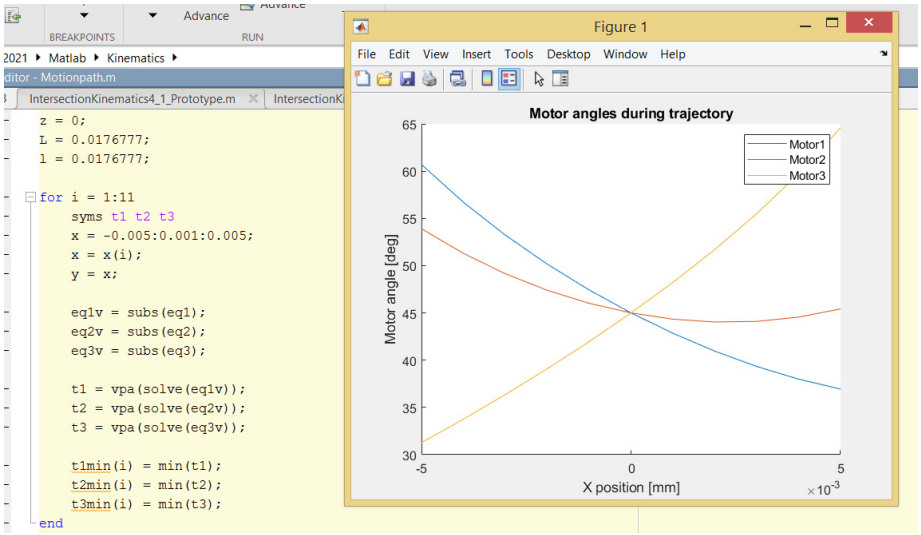

Figure 6.3: Motor angles necessary for a simple trajectory in x-direction

6.1.2 Jacobian

During the initial design phase, the valiability of the new mechanism was evaluated by finding the singular positions. As mentioned before, singular positions occur in a mechanisms workspace, and are

an undesired phenomenon. At a singular position, the behaviour of the mechanism can no longer be predicted, in other words, the input movement of the motors no longer dictate the output movement of the end-effector.

Finding the singularities of a fully constrained mechanism can be done using the Jacobian. The Jacobian is a matrix with all first-order partial derivatives of a function with multiple variables, in our case the kinematic equations mentioned above. Maple is a powerful software package that can derive equations with symbolic variables. Shown below in Figure 6.5 are the steps taken in Maple to evaluate the Jacobian.

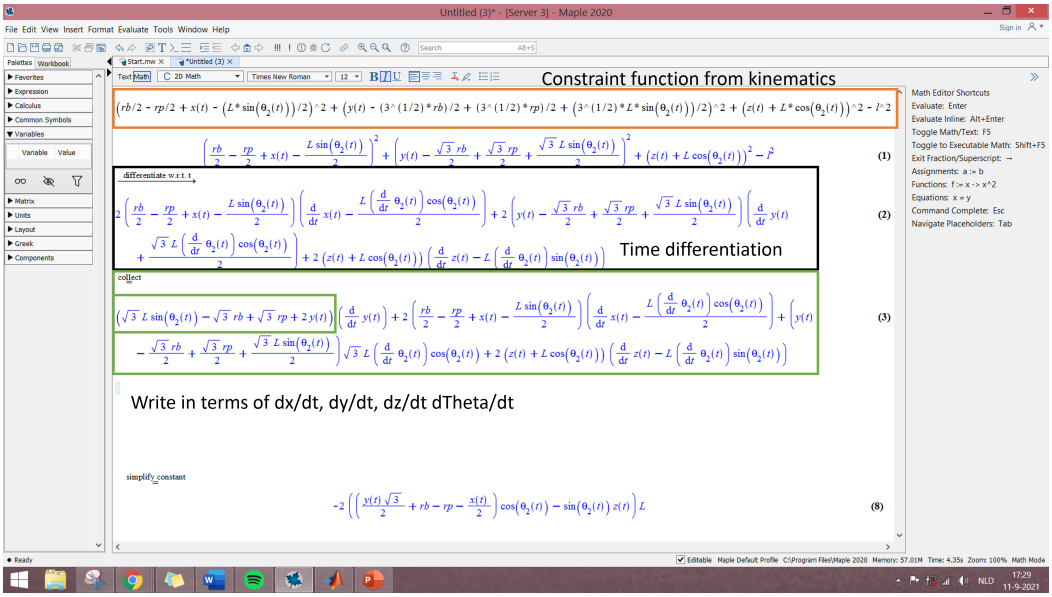

Figure 6.4: Evaluation of the Jacobian using Maple

Writing the results in the following form:

$$\mathbf{A}\dot{x} = \mathbf{B}\dot{\theta} \tag{6.1}$$

And taking the determinant of the A-matrix:

$$T = \begin{pmatrix} 2L\left(\cos\left(\frac{\pi t_1}{180}\right)(\mathrm{rb}-\mathrm{rp}+x)-z\sin\left(\frac{\pi t_1}{180}\right)\right) & 0 & 0 \\ 0 & -2L\left(z\sin\left(\frac{\pi t_2}{180}\right)-\cos\left(\frac{\pi t_2}{180}\right)\left(\mathrm{rb}-\mathrm{rp}-\frac{x}{2}+\sigma_1\right)\right) & 0 \\ 0 & 0 & -2L\left(z\sin\left(\frac{\pi t_3}{180}\right)+\cos\left(\frac{\pi t_3}{180}\right)\left(\mathrm{rp}-\mathrm{rb}+\frac{x}{2}+\sigma_1\right)\right) \end{pmatrix}$$

where

$$\sigma_1 = \frac{\sqrt{3}\,y}{2}$$

Figure 6.5: Evaluation of the Jacobian using Maple

The initial design to which this calculation was applied, was the fully constrained prototype with three arms. This design had equal upper and lower arm lengths. The rings were dimensioned so that, in its neutral position ($xyz = 0$), the arms had a relative angle of 90 degrees. Plugging these dimensional values in and equating that determinant to zero, results in three angles for the three motors. Namely:

$$\theta = 0, \pi/2, -\pi/2 \tag{6.2}$$

These are the angles for which the mechanism ends up in a singular position. The physical manifestation of these positions is discussed in the section on the first prototype.

6.1.3 Condition number

The condition number describes how sensitive the output of a function is to the change of the input. Applied to mechanisms, it measures the dexterity and the ability to change position or apply forces.

The condition number was used as a tool to select a suitable length for the upper and lower arms. To find the condition number for a certain position of the mechanism, the Jacobian is converted [1] and plugged into the condition number function of MATLAB. As an example, this calculation is applied to a trajectory of the device in x-direction. The resulting plot is shown below in Figure 6.6. Here, the different lines represent different arm lengths.

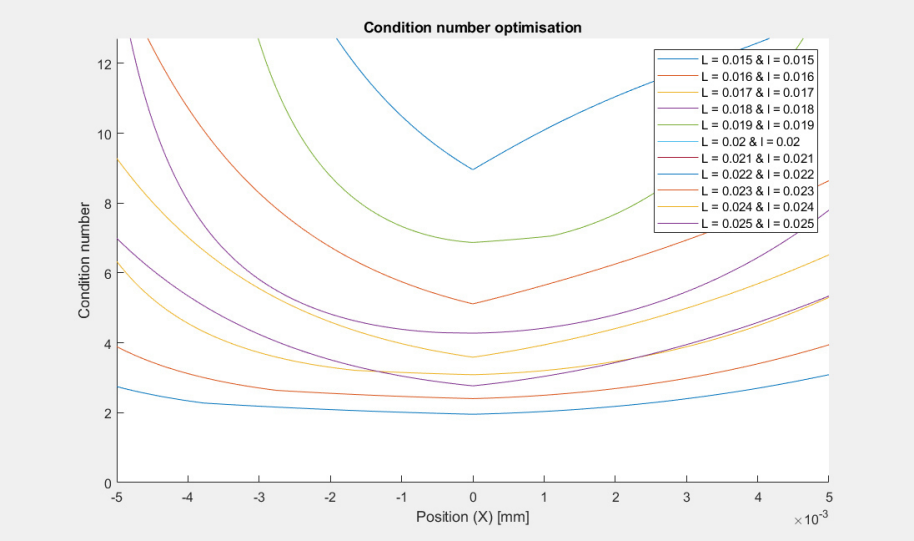

Figure 6.6: Condition numbers for a trajectory with different arm lengths

A condition number of 1 means the best force transmission possible. In this example corresponding to certain inner and outer ring dimensions, the arm length of 20mm has the lowest condition number while moving through the workspace. One can imagine that the condition number decreases when the

[1] Merlet, J. P. (June 20, 2005). "Jacobian, Manipulability, Condition Number, and Accuracy of Parallel Robots." ASME. J. Mech. Des. January 2006; 128(1): 199–206.

mechanism moves to the limits of the workspace, since the position of the arms become less advantageous. This effect can also be seen in Figure 6.6.

6.2 Simulink simulation

6.2.1 Intersection method for kinematics

The previously mentioned method to determine the kinematics is computationally demanding. For simulation, optimization and experiments, many trajectories have to be calculated. The trajectories themselves consists of a large amount of setpoints, that are determined by the inverse kinematics. Therefore, the method to derive the kinematic relation used throughout the project is chosen to be a computationally less demanding one [2][3](geometric).

The freedom of movement of the 1DoF rotational constraint provided by the servo motor can be represented by a circle. For the balljoints, this degree-of-freedom is represented by a sphere. The intersection between the two is a geometric equation, and can be used to relate the motor angle to the position of the end-effector.

The first step is to define all the necessary dimensional parameters, together with the desired trajectory (e.g. -0.005 to 0.005mm). The signal is determined by the acceleration profile and magnitude. In our experiments, a block wave was used most. In the algorithm, the magnitude is selected and the motion path is determined by calculating back from the acceleration profile. This motion path is then split up in discrete sections, by making use of the Nyquist criterion for sampling. An illustrative representation of this is shown in Figure 6.7.

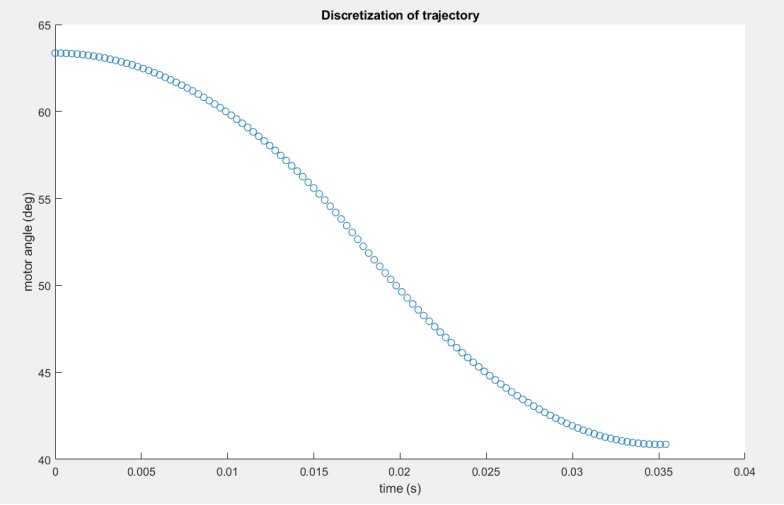

Figure 6.7: Example of discretization of angular motor input

[2]https://math.stackexchange.com/questions/256100/how-can-i-find-the-points-at-which-two-circles-intersect
[3]https://robotics.stackexchange.com/questions/3144/inverse-kinematics-of-parallel-manipulator-delta-robot

In a loop, the trajectory with discrete position steps is then converted to motor angles. Each loop uses a different rotation matrix to obtain the angles for each motor. This part of the algorithm is shown in Figure 6.8 below.

```
for j = 1:1:timeStep
    xPos = xyzTraj(1,j);
    yPos = xyzTraj(2,j);
    zPos = xyzTraj(3,j);
    B = [xPos;yPos;zPos];
    for i = 1:4         % Fuction to determine the motor angles
        transMatback = [cosd(th(i)) -sind(th(i)) 0; sind(th(i)) cosd(th(i)) 0; 0 0 cosd(2*th(i))]; % added cosd(2*th(i)) for z
        transMatfor = [cosd(-th(i)) -sind(-th(i)) 0; sind(-th(i)) cosd(-th(i)) 0; 0 0 1];

        Bjoint = transMatback*(B + transMatfor*[rb;0;0]);
        Pjoint = transMatback*(P + transMatfor*[rp;0;0]);

        rInt = sqrt(l^2 - Bjoint(2)^2);

        R = sqrt((Bjoint(1)-Pjoint(1))^2 + (Bjoint(3)-Pjoint(3))^2);

        xInt(1) = 1/2*(Pjoint(1)+Bjoint(1)) + ((rInt^2-L^2)/(2*R^2))*(Bjoint(1)-Pjoint(1)) + 1/2*sqrt(2*((L^2+rInt^2)/R^2) - (
        xInt(2) = 1/2*(Pjoint(1)+Bjoint(1)) + ((rInt^2-L^2)/(2*R^2))*(Bjoint(1)-Pjoint(1)) - 1/2*sqrt(2*((L^2+rInt^2)/R^2) - (
        zInt(1) = 1/2*(Pjoint(3)+Bjoint(3)) + ((rInt^2-L^2)/(2*R^2))*(Bjoint(3)-Pjoint(3)) + 1/2*sqrt(2*((L^2+rInt^2)/R^2) - (
        zInt(2) = 1/2*(Pjoint(3)+Bjoint(3)) + ((rInt^2-L^2)/(2*R^2))*(Bjoint(3)-Pjoint(3)) - 1/2*sqrt(2*((L^2+rInt^2)/R^2) - (

        motorAngle(i,:) = [atand((zInt(1)-Bjoint(3))/(Bjoint(1)-xInt(1))), atand((zInt(2)-Bjoint(3))/(Bjoint(1)-xInt(2)))];

    end
    trajectory(j,:) = motorAngle(:,2);
end
```

Figure 6.8: Geometric approach to inverse kinematics

The output of the loop is a matrix with angular positions for each motor. This data is modified multiple times in successive steps. For the Simulink simulation, a time signal is added to the matrix. For experiments, the angles are converted to a pulse width (PWM), which is the input format of the servo motor. The matrix is also converted into individual arrays for the Arduino to process.

Additional checks are also part of the MATLAB code. The ball joints have a maximum rotation in one degree-of-freedom, namely 25 degrees in both directions. The servo motors have a maximum angular velocity, which was empirically determined to be 920 deg/s. The code gives a warning if, during the computation of a trajectory, these limits are reached.

It was not anticipated that the seemingly fast servo motors would provide such a limitation to the system. In Figure 6.9 the different lines each represent the length of the stroke of the outer ring. The horizontal line is the limit of the angular velocity. From this figure, it can be seen that for a perturbation of around 5N, a maximum stroke of 6mm is possible. Which means that a longer sustained pulse of 5N is not achievable. Most experiments are done with a stroke of maximum 10mm, which means that the full stroke capacity of the mechanism is not utilized and the mechanism plus the outer ring could be designed more compact.

6.2.2 Simulink model

The mechanism was modelled in Simulinks simscape package to gain knowledge on the behaviour of the system. The design is simplified, but important dimensional and inertial parameters are matched.

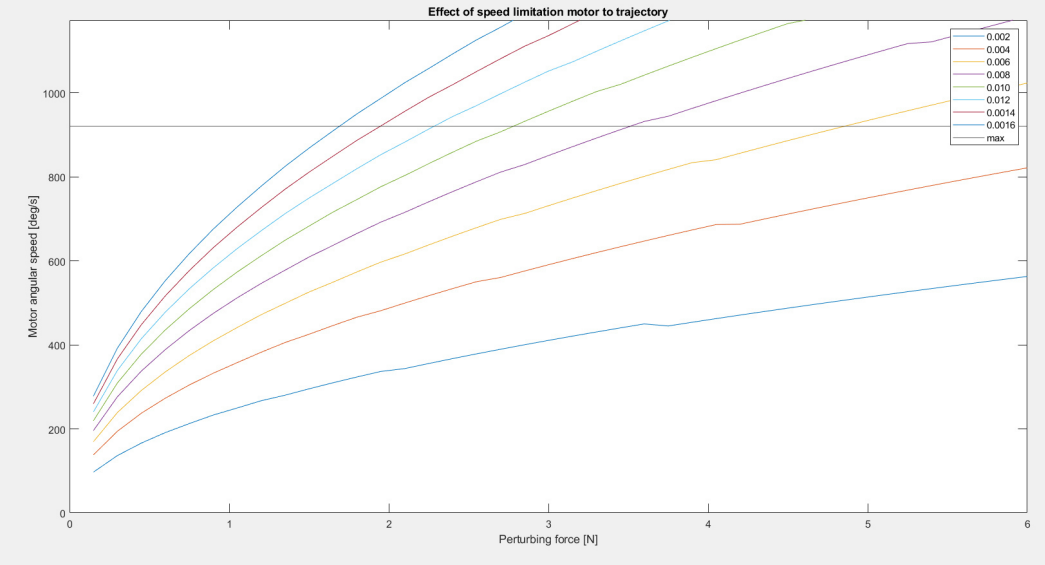

Figure 6.9: Travel and perturbation force limited by motor speed

The model makes use of the previously discussed MATLAB algorithm. The columns of the trajectory matrix are split up and used as an input for each of the four motors. The building blocks of the model are shown in Figure 6.10. Since the mechanism is overconstrained, initially the simulations solver had trouble converging. This was solved by replacing a driven rigid arm by compliant one. The stiffness of this member was set adequately high, so that it would not change the dynamics of the system, yet allow the configuration to be solved.

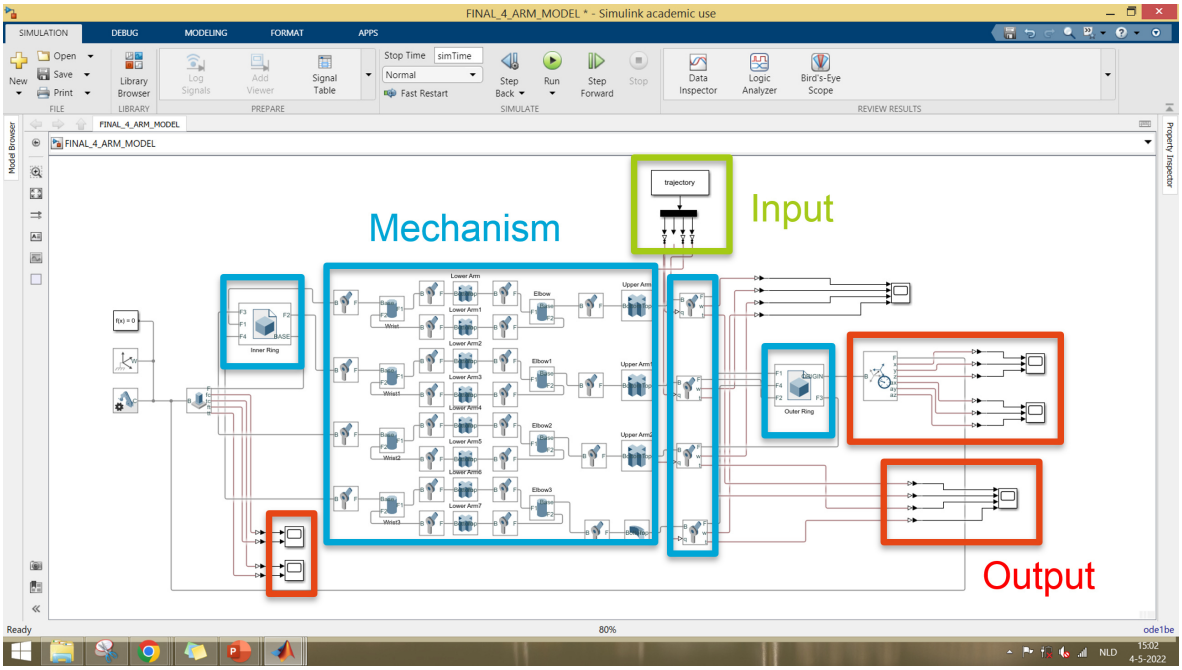

Figure 6.10: Parallel mechanism modelled in simscape

Sensors (scopes) are placed on various components of the mechanism. They are marked as output in Figure 6.10. The sensors on the outer ring can be used to plot the respective displacement, velocity and acceleration. The acceleration multiplied by the mass simulates the force signal that is used for the perturbation. The perturbing signal used as example has the following parameters: travel is -0.005 to 0.005mm, block wave with acceleration of 32 m/s. Figure 6.11 shows signals displayed by the scope connected to the outer ring. Here, the relative position of the outer ring and its acceleration are plotted against the time.

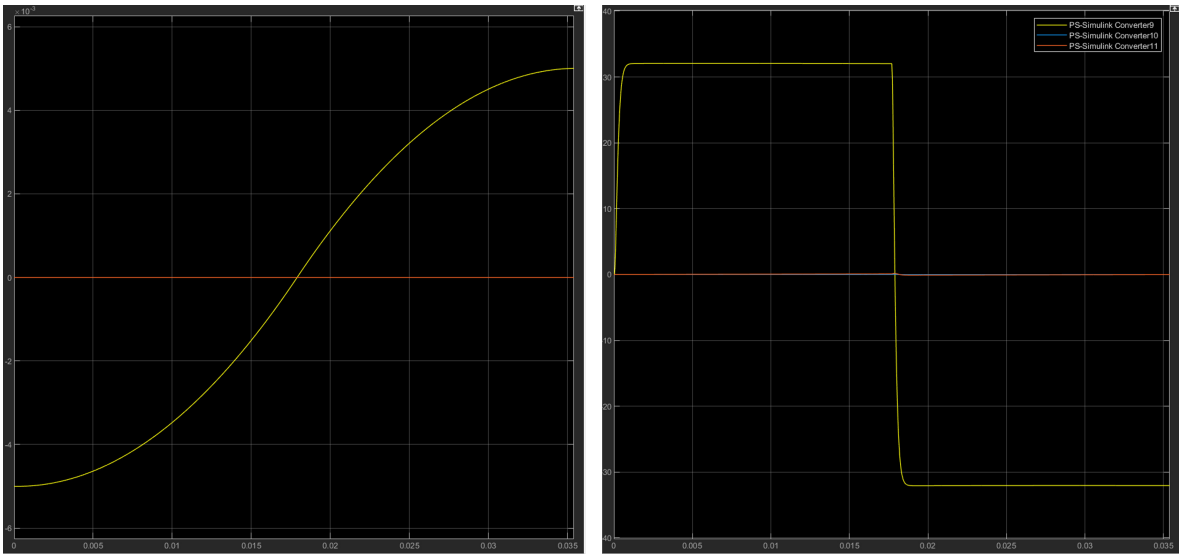

Figure 6.11: Position (left) and acceleration (right) of end-effector (outer ring)

As been discussed before, the input for the motors are discrete angle positions. The same input is given to the simulation. A trajectory is chosen and with inverse kinematics the angles are calculated. It is hard to find out what motor specifications are required to generate the desired motion. With the Simulink simulation it is possible to put a torque sensor on the joints that represent the motors. The left plot in Figure 6.12 shows the angular velocity of all four motors during the trajectory. The plot on the right is the torque profile. With these two diagrams it is possible to select the right motor for a specific perturbing signal.

Other useful data that was extracted from the simulation, were all the theoretical reaction torques and forces. These can be seen in Figure 6.13. Since the device is designed to be used as a tool for system identification, the goal was to create a distinct force perturbation in one direction, while the reaction forces and torques in other directions were kept to a minimum. The way the mechanism is oriented allowed for the ring to move co-planar, inducing little reaction torques. The members of the mechanism have negligible inertia compared to the moving mass, keeping the theoretical parasitic forces that are generated low. By simulating a model of your system, it is possible to check the functioning of the mechanism, choose the right actuator, and optimise for low parasitic forces and torques.

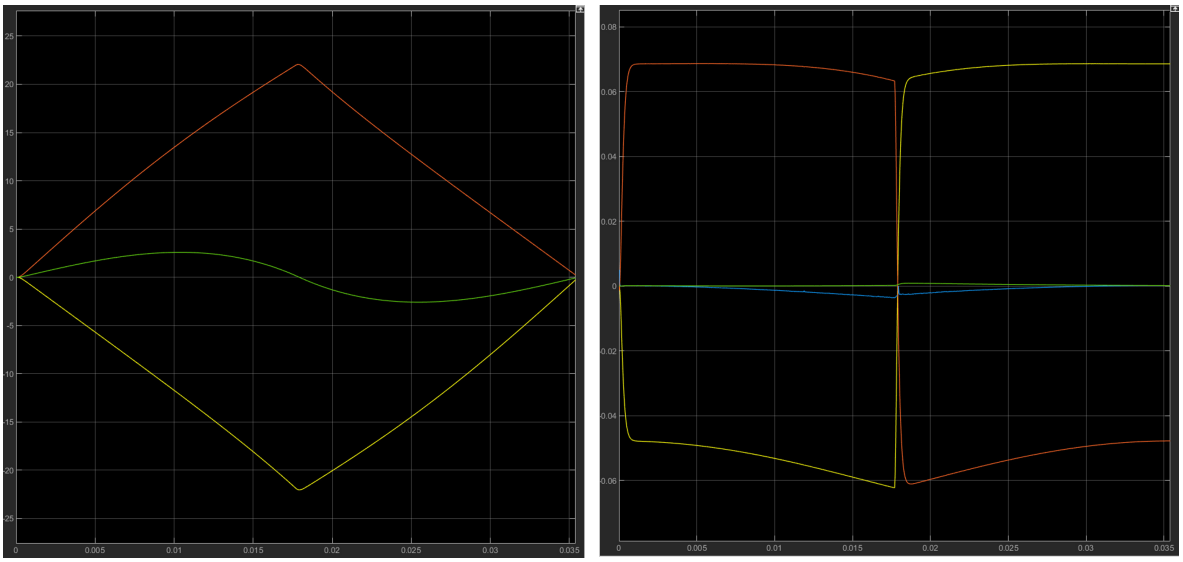

Figure 6.12: Position (left) and acceleration (right) of end-effector (outer ring)

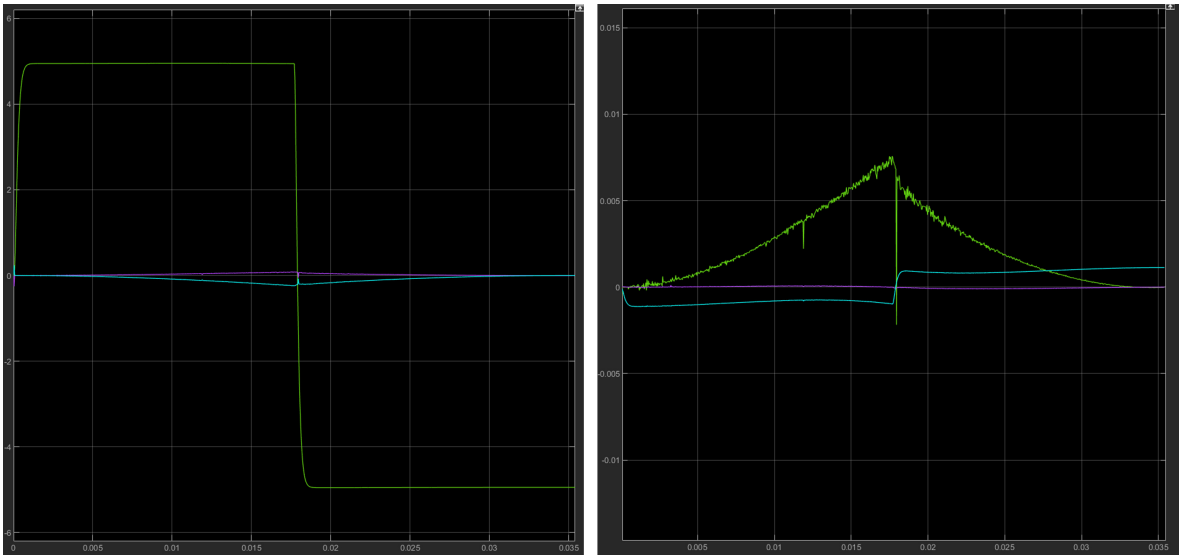

Figure 6.13: Reaction force (left) and torque (right) on the base (inner ring)

6.3 First Delta prototype and production

6.3.1 Actuator selection material

The selection of actuator and mechanism go hand-in-hand. Properties of the actuator like their degrees-of-freedom, power and dimensions, determine which mechanism can be used. During the design process, while converging to a parallel mechanism, six different actuators remained. Two linear electric actuators and four electric motors.

In Figure 6.14, the main performance specifications are compared. Since the perturbator is meant to

be a non-intrusive wearable device, mass and volume were important parameters to consider. Therefore, some specifications of Figure 6.14 only become relevant once scaled with mass or volume. This is shown in Figure 6.15. Other properties of the different actuators, like cost, off-axis load capability, and required auxiliary power electronics, were also considered in the selection.

Performance comparison

Actuator type	Continuous force/torque (Holding)	Positional accuracy	Speed	Mass	Voltage
DS215MG (Servo)	--- (0.363) Nm	0.5°	200 rpm	20 g	7.4 V
CHIHAI MOTOR DC6V 90RPM N20 (DC Gearbox)	0.068 (0.147) Nm	1.81° (Improves with better encoder)	90 rpm	20 g	6 V
N20 DC12V	0.196 ( ) Nm	AS5600: 0.35°	90 rpm	20 g	12 V
PM2205 (Direct drive)	0.04 (0.06) Nm	0.35°	792 rpm	20 g	12 V
SDLM-019-070-01-01 (Linear Direct)	2.0 (6.4) N	1.25 um	Unspecified	91 g	Unspecified (control dependent)
GVCM-019-022-02 (Voice coil)	2.3 (7.4) N	Encoderless	Unspecified	35 g	Unspecified (control dependent)

Figure 6.14: Important performance parameters of actuators

Power density

Actuator type	Continuous Power	Power density (volume)	Power density (mass)	Force/Torque density (volume)	Force/Torque density (mass)	Volume mm^3	Mass (g)
DS215MG (Servo)	7 W	0,93	0,35	0,0484	18,2	7502	20
CHIHAI MOTOR DC6V 90RPM N20 (DC Gearbox)	1 W	0,27	0,05	0,0186	3,4	3660	20
PM2205 (Direct drive)	8 W	0,74	0,4	0,0037	2	10756	20
SDLM-019-070-01-01 (Linear Direct)	6 W	0,3	0,07	0,32	70,3	20027	91
GVCM-019-022-02 (Voice coil)	5 W	0,65	0,14	0,96	211	7735	35

Figure 6.15: Specifications scaled by mass or volume

6.3.2 Production

The main concern with the design of the arms, was the trade-off between precision, stiffness, and size. Finding off-the-shelf universal joints that suited the scale of the mechanism turned out to be a problem. Therefore, it was decided to use hobby grade ball joints (Figure 6.16). These offered a simple and low friction solution. Having M2 threaded holes, allowed us to turn two of them into a solid arm by using a piece of threaded rod. In hindsight, these ball joints were not designed for a precision application, introducing considerable play.

To complete the parallelogram of the lower arm, two types of shafts were produced on the lathe. The 'wrist' shaft interfaces with the inner ring. The 'elbow' consists of two smaller shafts that connect the upper arm with the lower arm. Brass was used since it is easy to machine on this scale, but also provides ample stiffness. The shafts had M2 threaded holes tapped into them. The whole assembly, including the servo motors were fastened with M2 bolts.

Figure 6.16: Off-the-shelf micro ball joints

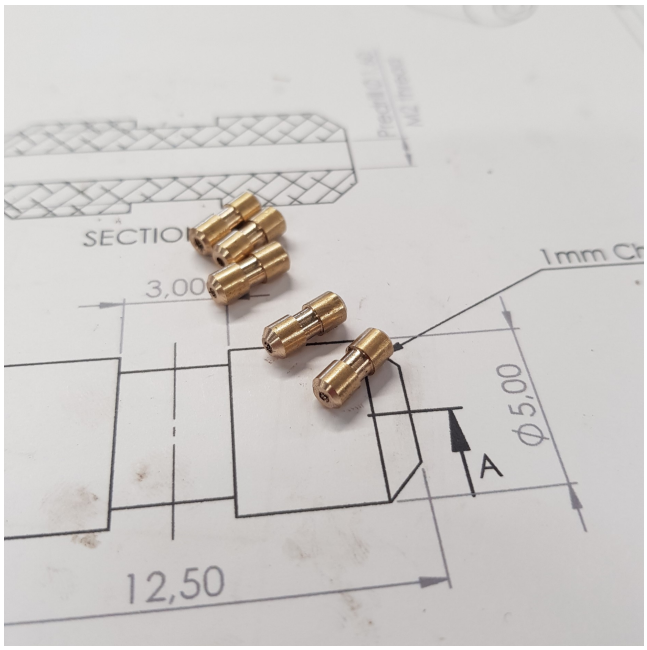

Figure 6.17: Turned and tapped brass shafts

Servo motors have a specific splined output shaft, which makes it hard to produce a custom arm. Therefore, you are bound to use off-the-shelf components. Provided with the servo's are plastic arms that offered little stiffness. Some replacement aluminium arms were used instead. The assembly that forms the upper and lower arms of the mechanism is shown in Figure 6.18.

6.3.3 First prototype

Before ordering the servo motors and ball joints, a basic proof-of-concept was created with 3D printed parts and paperclips as hinges. This gave sufficient proof that the real mechanism would have potential.

Figure 6.18: Upper and lower arms of the mechanism

The initial design, with three arms, can be seen in Figure 6.19.

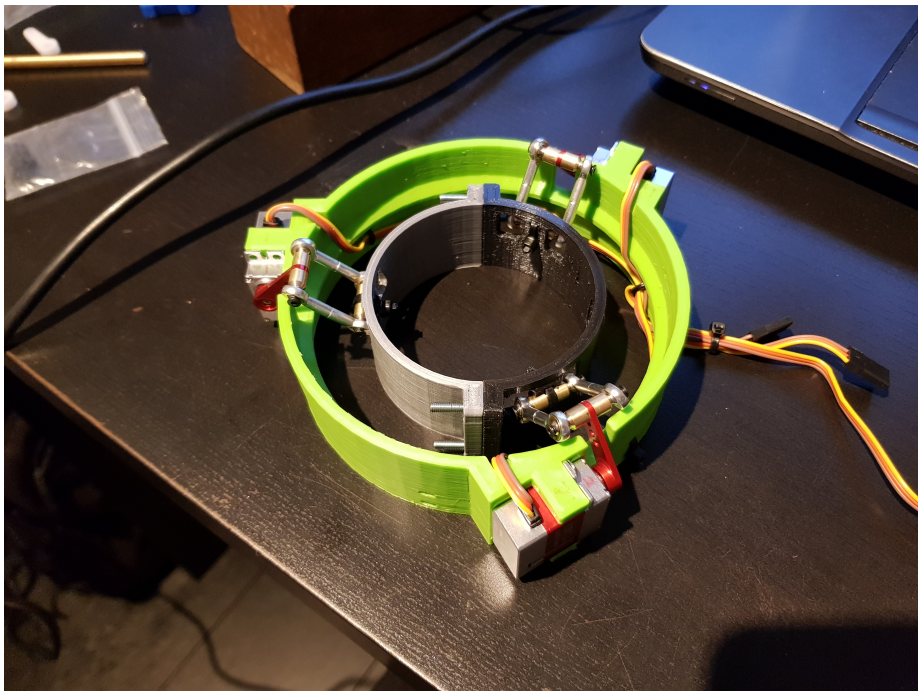

Figure 6.19: First prototype with new mechanism

The first few tests looked promising. Here, the device was supported at the outer ring, while the inner ring smoothly moved trough the workspace. However, when supported at the inner ring, the outer

ring was subjected to gravity. While the device was repeatedly doing a back-and-forth sweep in-plane, the inner ring was moved around and rotated, just like it would have during the real world application. Near the limit of the workspace, where stiffness is the lowest, the outer ring started to rotate and lose its parallel position with respect to the inner ring. Even though the members were not placed in their singular positions, which were determined earlier, the mechanism still lost its rigidity. Due to the play present in the ball joints, the mechanism was too sensitive to end up in the singular positions. The loss of parallelism and rigidity in a singular position is displayed in Figure 6.20.

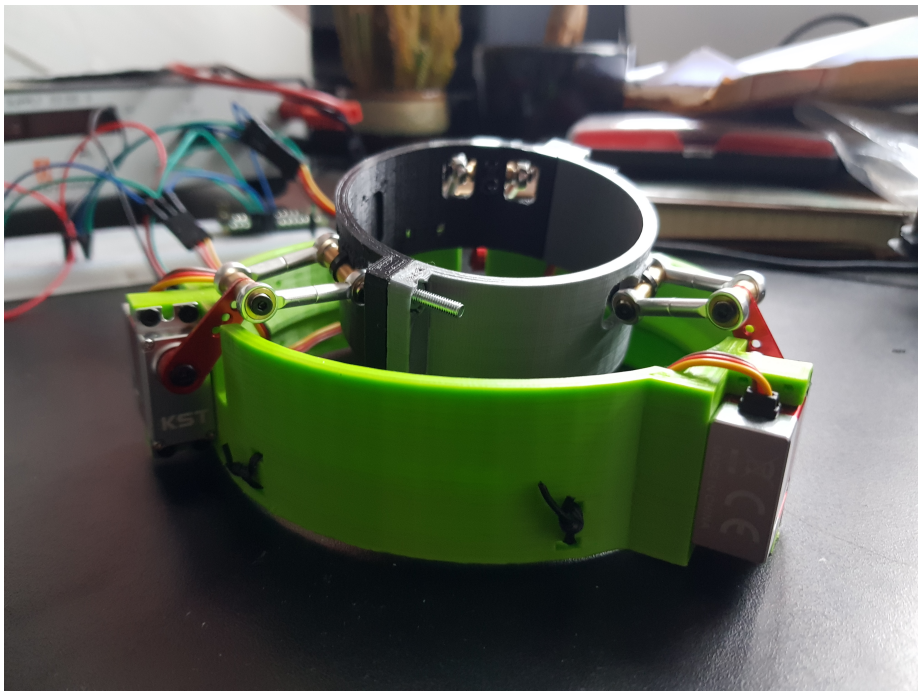

Figure 6.20: Loss of parallelism due to singularity

The scope of this project was to generate the ungrounded input signal for system identification. However, a sensor suggestion to measure the output was implemented in the first prototype (Figure 6.21).

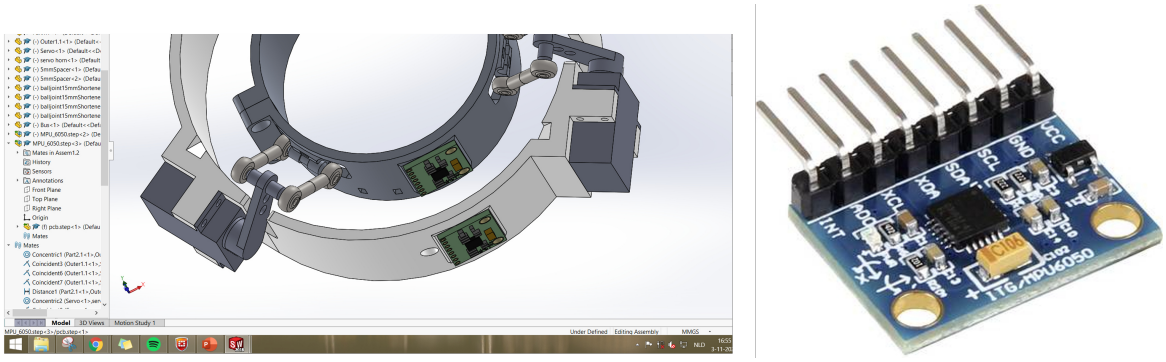

Figure 6.21: Dual accelerometer for system identification

6.4 Final design

6.4.1 Features

Since the device is meant to be mounted on the human wrist, this is taken into consideration during placement of the mechanism. The inner ring is able to split by undoing two fasteners. The arms of the mechanism can then moved out of the way and the device can be (dis)mounted on/from the arm. In Figure 6.22 the two parts of the inner ring have different colors. The inner ring has an inside diameter of 65mm, accommodating most wrists. It is envisioned that moulded inserts are created to provide a tight fit with the wrist. Each of the two halves of the inner ring has a small protruding pin, meant to create a form-fit with the moulded inserts.

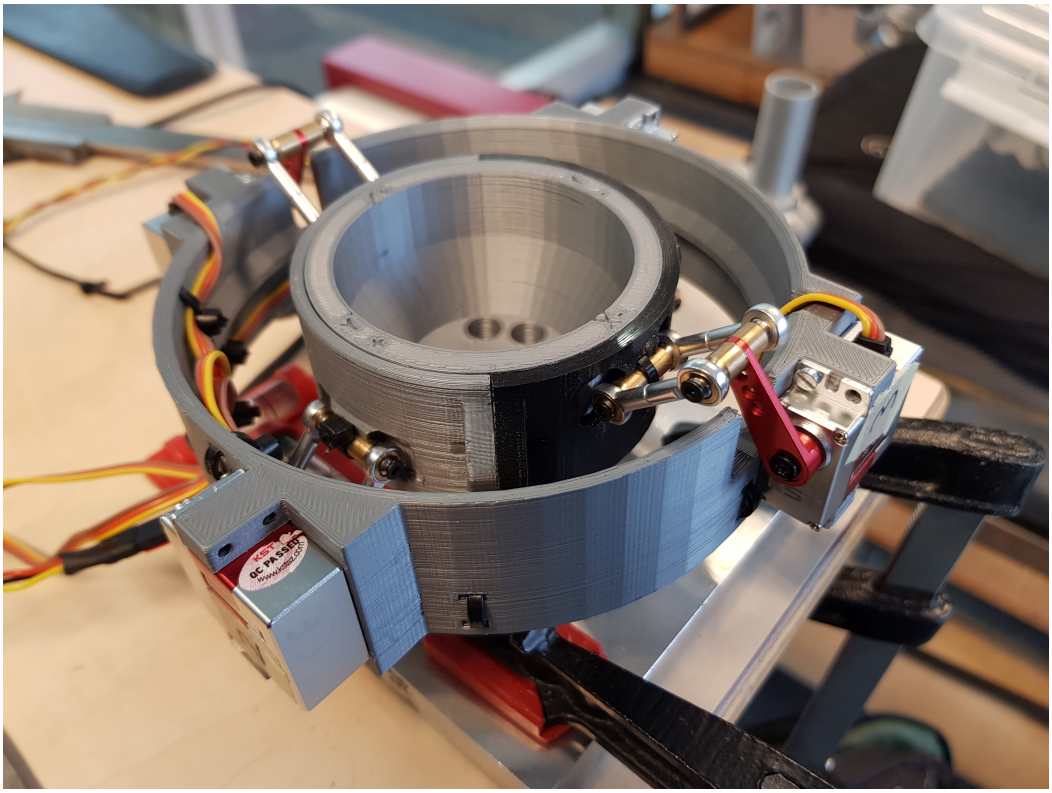

Figure 6.22: Prototype on test setup with the two piece inner ring

Three possible arm orientations were considered while designing the second iteration of mechanism. A simple drawing of the options in a singular positions is shown in Figure 6.23. The left option gained three additional degrees-of-freedom. Translations in the direction of the arrows, and a rotational degree-of-freedom represented by the dashed line. The middle option also gained a rotational degree-of-freedom. The third orientation was selected for the re-iteration. It still has singularities at the limit of the workspace, however it is estimated to be less sensitive while performing (near) in-plane trajectories than the other options.

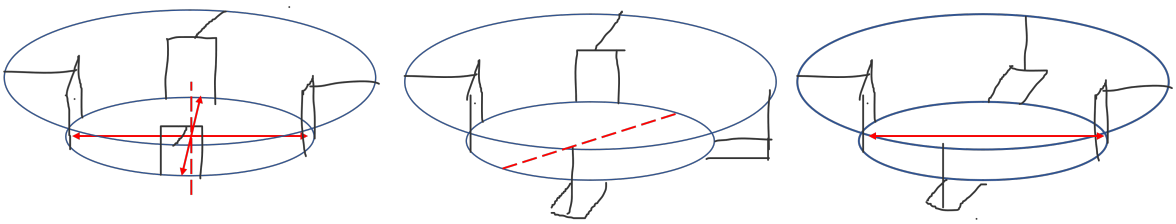

Figure 6.23: Three possible redundant arm orientations

6.4.2 Arduino and electronics

From the trajectory planning algorithm in MATLAB, the motors angles were already in a format that the servo could use. Four arrays of angle data were uploaded to the Arduino's internal memory. When power is applied to both the Arduino and the prototype, the outer ring stays in its neutral position, at $(x, y, z) = (0, 0, 0)$. After a timeout, a for loop takes the first entry of the four arrays and writes them to the servo motors. After that, the successive entries, with a delay matching the generated trajectory, are written to the motors. The for loop keeps repeating until the power is shut down.

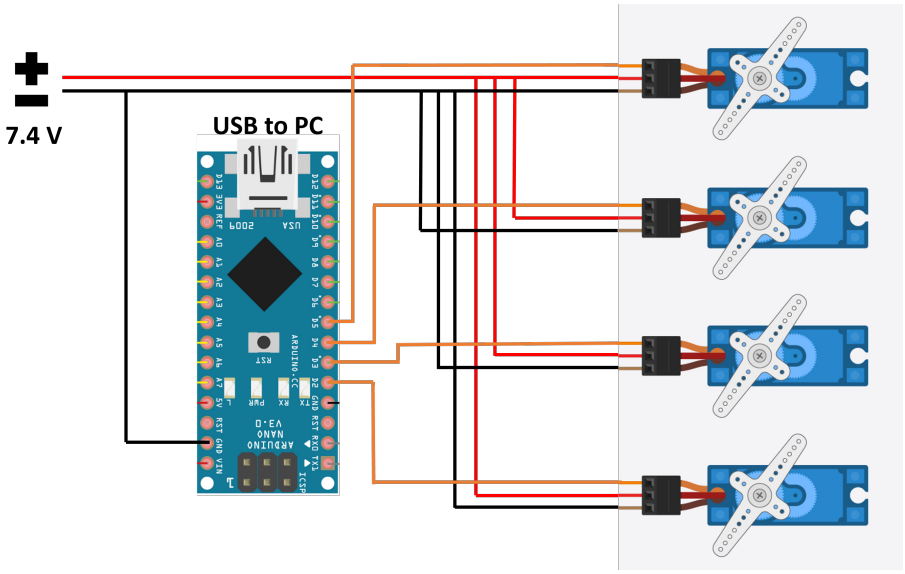

Figure 6.24: Basic wiring of the electrical components

Figure 6.25 shows how the motors and Arduino were wired during the experiment. The 7.4 volts came from an adjustable power supply. The Arduino got its power from the USB connection, however it could share its power supply with the motors. For the motors to function correctly, the motors and Arduino needed to have a common ground. When used as a perturbing device in daily life, the 7.4V can be supplied by a two cell lithium-ion battery. This is a compact power source, which can power the device at 100% duty cycle for roughly an hour.

6.4.3 Technical drawing

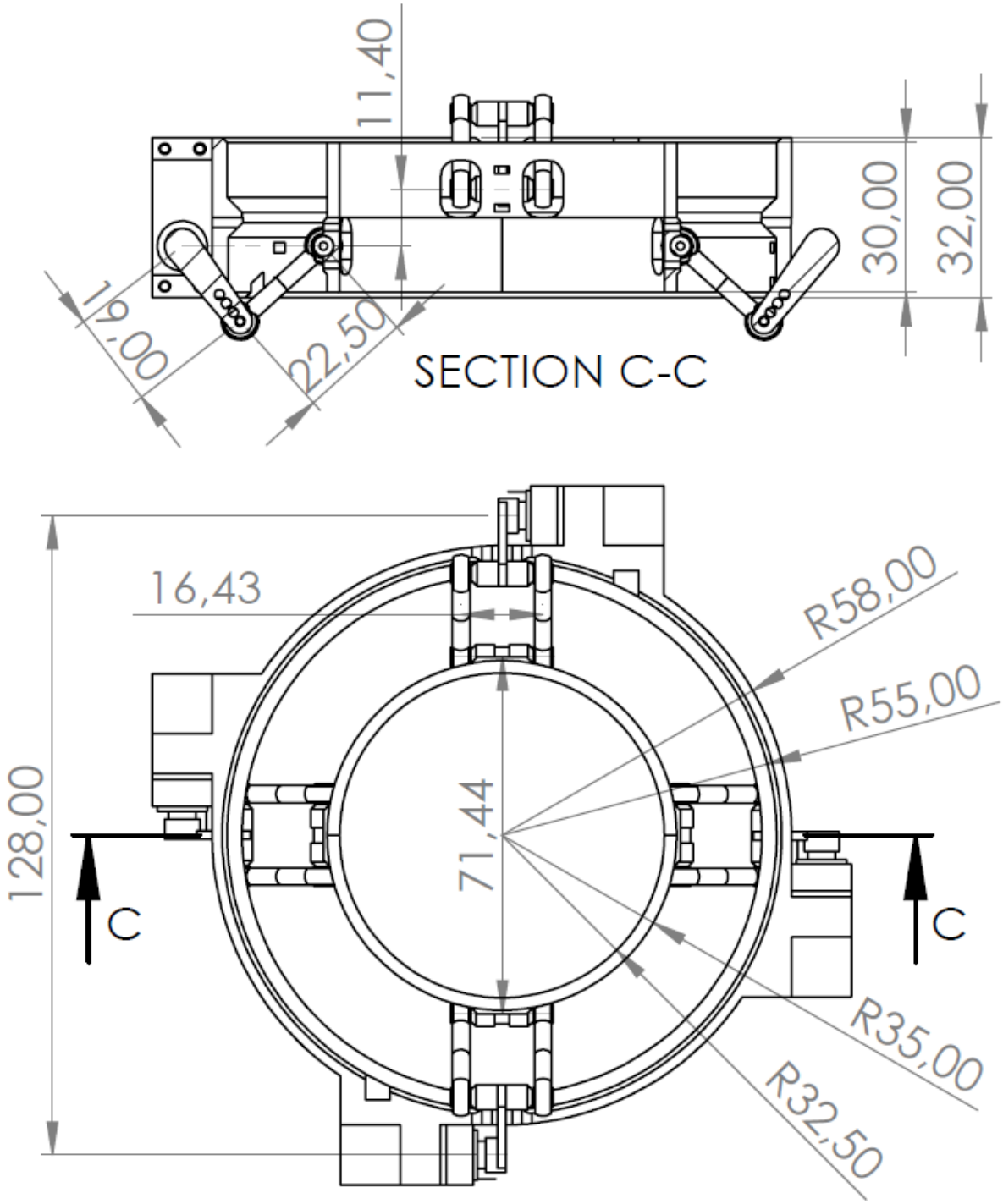

Figure 6.25: Technical drawing with most important dimensions

6.5 Experiments and setup

6.5.1 Setup

Figure 6.26 shows the ATI mini45 force and torque sensor as it was used in the experiments. It is mounted to a aluminium backplate, which was levelled and clamped to a table. An adapter was 3D printed to make a sturdy connection between the prototype and the force sensor. In the paper, results are shown for measurements with the prototype both parallel to the table and 90 degrees rotated. This was done to validate whether the device would work repeatably in different directions, which is realistic during use in daily life. Figure 6.27 shows the measurement setup of the rotated experiments.

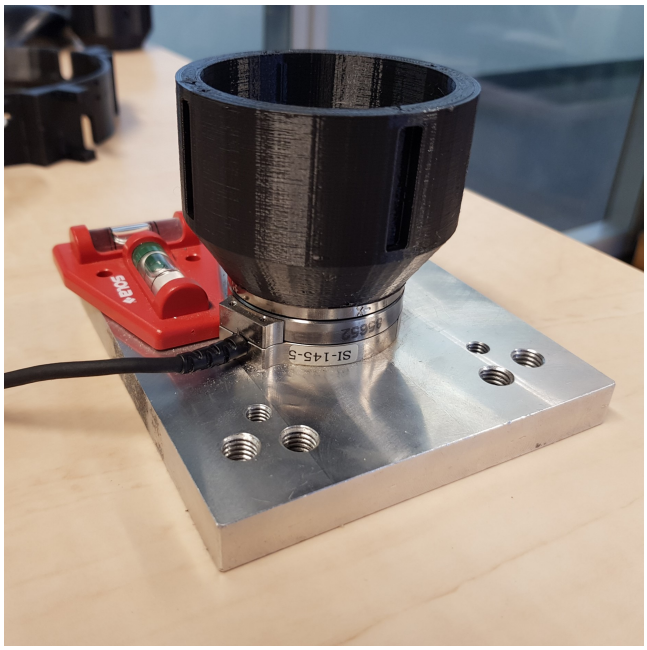

Figure 6.26: Sensor setup with adapter

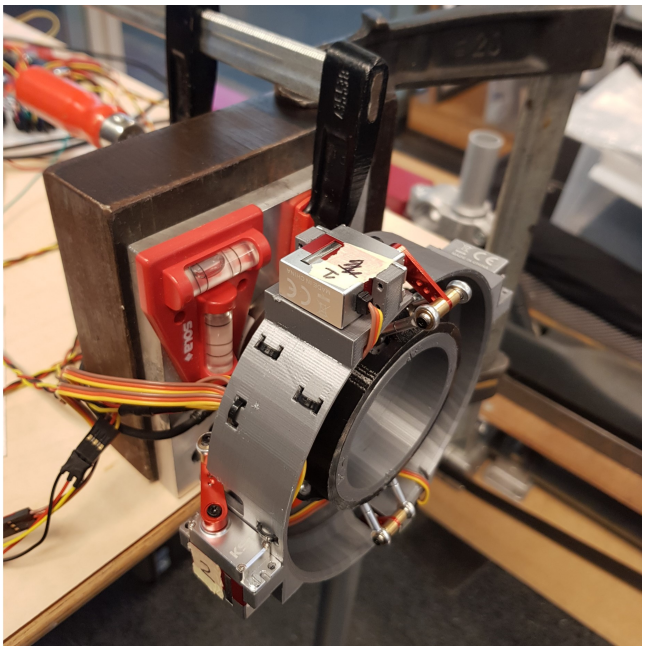

Figure 6.27: Setup 90 degrees rotated

6.5.2 Additional experiments

The servo motors that power the prototype are normally used in hobby applications. Here, the trajectory between setpoints is not important. Before committing to the servo motors, a validatory test was performed to check whether they were able to follow a given trajectory. This was done with a 1DoF setup, where the motor is attached to a linear guide (Figure 6.28 & 6.29). The mechanism design resembles one of the arms of the prototype. An extra mass attached to the arm for added non-linearity.

The different motor trajectories were taken from the MATLAB kinematics script. In one of the experiments, the servo had to move 15mm in 0.1s. To measure how closely the motor was able to follow the given trajectory, a hall encoder was used. The results of one of the tests can be seen in Figure

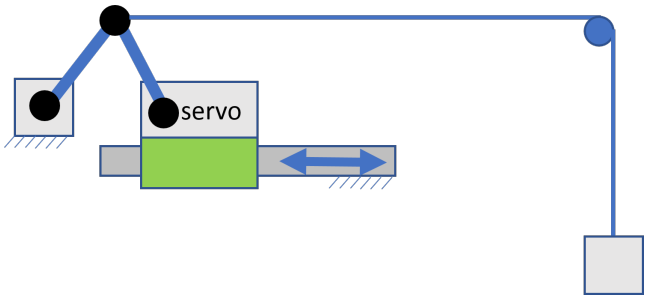

Figure 6.28: Schematic overview

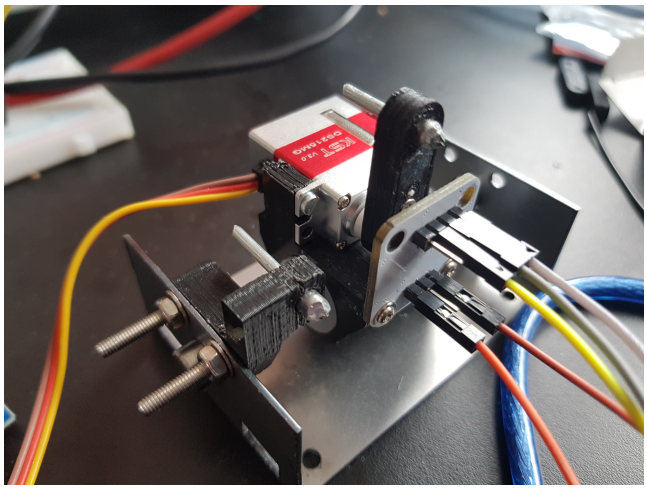

Figure 6.29: 1DoF test setup

6.30, where the goal trajectory is plotted against five measurements. The outcome of the different experiments gave confirmation to continue with the servo motors.

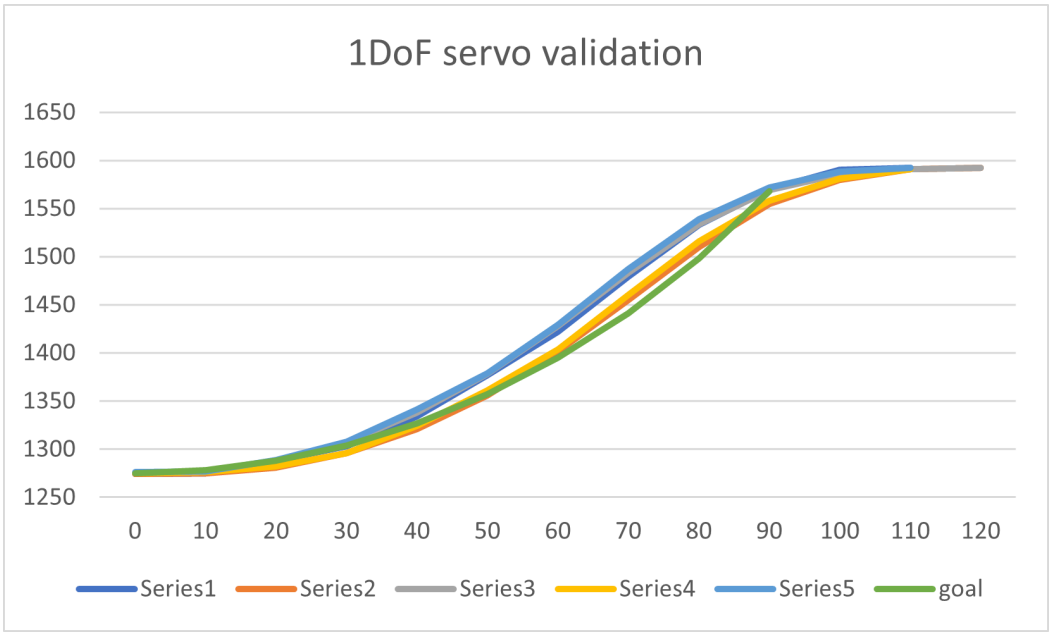

Figure 6.30: Results of 1DoF validation experiment

Setpoint tracking has been a problem during the experimental validation of the design. From the moment that the fluctuations in the signal were observed, experiments were done to pinpoint the source. The number of discrete setpoints was increased in the first test. But since the resolution was already sufficiently high, this had no significant effect. Figure 6.31 shows the measured force signal with the trajectory split up into 10, 20 and 80 steps, respectively.

The second experiment to find the source of the rocky signal, was related to the maximum speed of the motors. To find the maximum speed of the motors, a periodic trajectory from -0.004 to 0.004mm

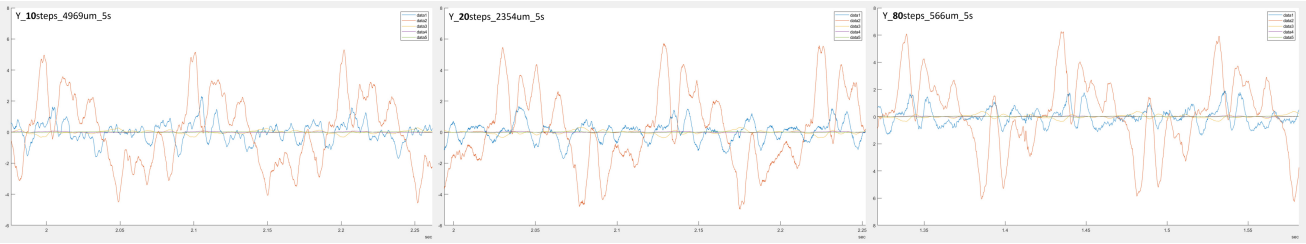

Figure 6.31: Set point resolution: 10 (left), 20 (middle), 80 (right)

was repeated with increasing acceleration (see Figure 6.32). At some point, the signal no longer reached its desired magnitude. This was at a force magnitude of 4N and motor speed of 32rad/s. However, even though all future experiments were performed below that speed limit, the dips still remained in the signal. Note that the scaling in the images are not exactly the same, they are solely meant as illustration of the problem.

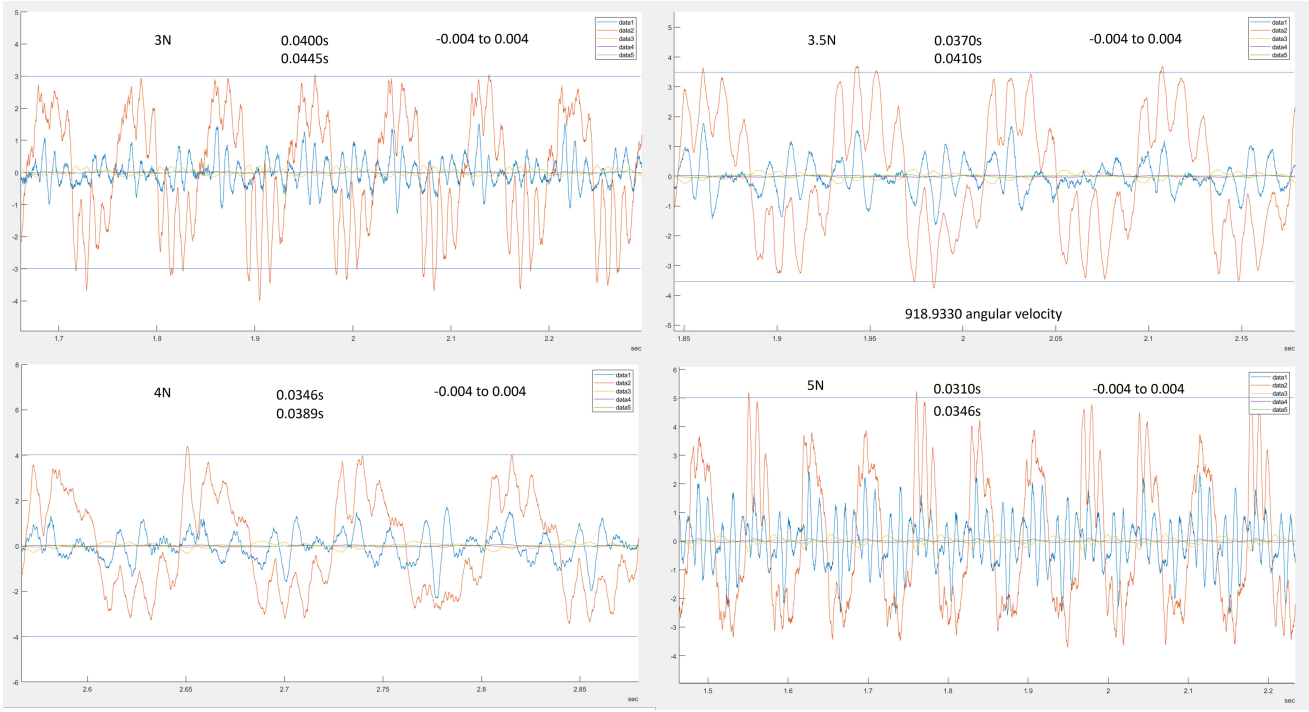

Figure 6.32: Finding the maximum loaded motor speed

Play in the ball joints or low stiffness of 3D printed components could be the culprit behind the poor setpoint tracking. However, when looking closely at the generated force signals, this also is not probable. To understand this, it is important to imagine what the mechanism and the outer ring are physically doing at certain points in the trajectory. To make this more clear, two lines are placed in Figure 6.33. These lines indicate the position at which the outer ring is at its travel limit and changes direction. Here, the outer ring goes from being decelerated to being accelerated, with the resultant force pointing in the same direction. In the middle between the two lines, the outer ring goes from

being accelerated to being decelerated, here the force changes sign. The most noticeable effect of play or flexibility is expected here. However, the dips also occur when not in these 'special positions'. Therefore, it is not expected that play or lack of stiffness is the main contributor to this problem.

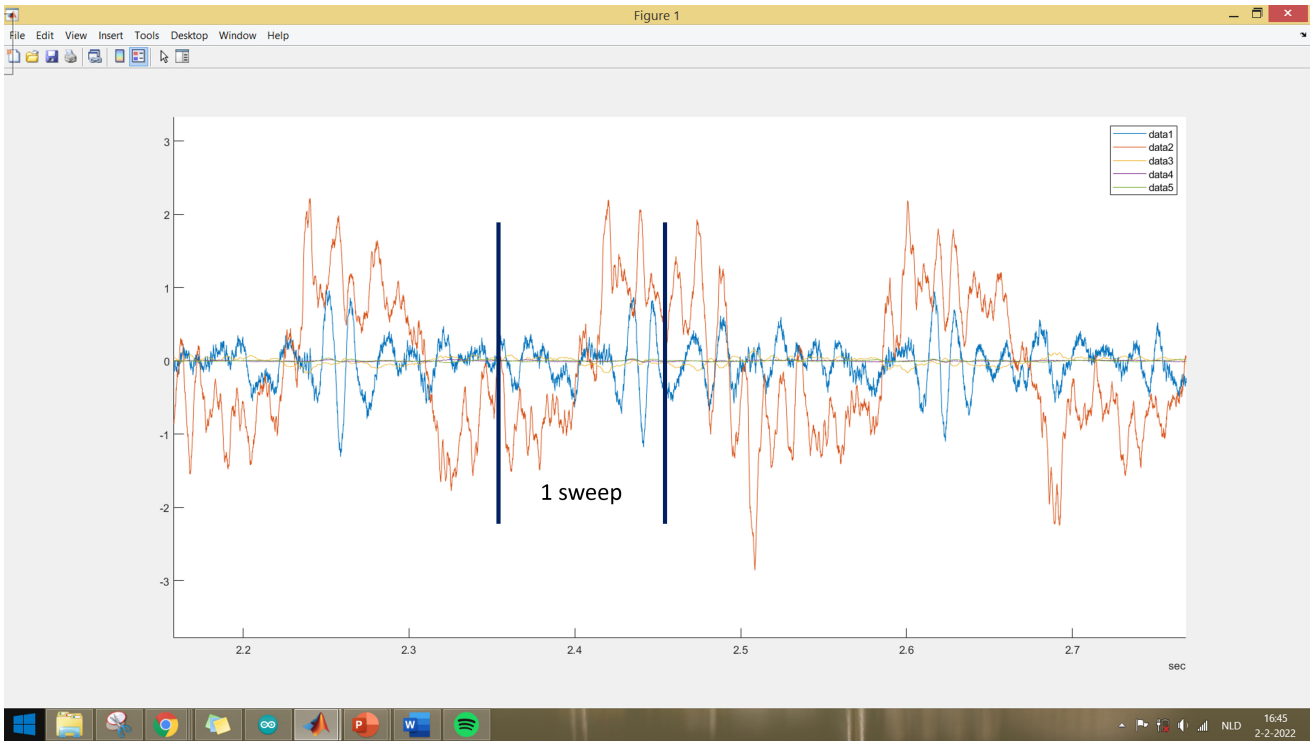

Figure 6.33: Physical meaning behind the perturbing force signal

By incrementally adding more mass to the outer ring (Figure 6.35), the acceleration can be decreased to achieve the same perturbing force (3N). The controller of the servo, which is has a relatively low frequency of 333Hz, is then able to use more setpoints for the same trajectory. This is important, since the redundancy might cause the motors to oppose each other in between setpoints. With added weight, the signal gets increasingly smoother (Figure 6.34). Since the dips smooth out during the discussed experiments, they are expected to be the result of a slow and poorly tuned controller.

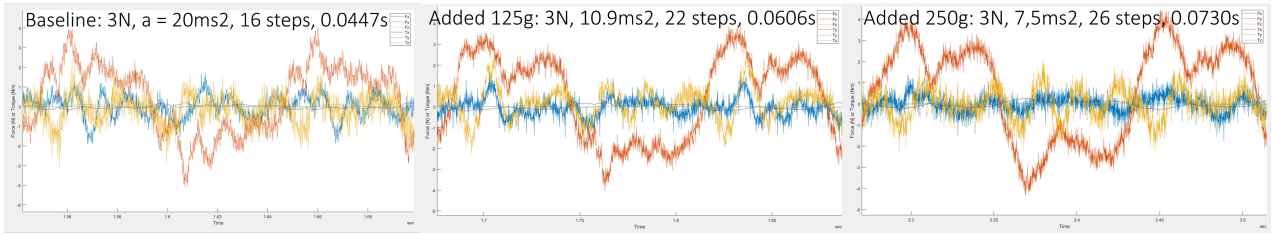

Figure 6.34: Increase of moving mass: Baseline (left), 0.125kg added (middle), 0.25kg added (right)

During the experiments to find the reason behind the rough signal shape, we were able to produce a relatively smooth perturbing signal with a magnitude of 8N (Figure 6.36). This is a result of the added

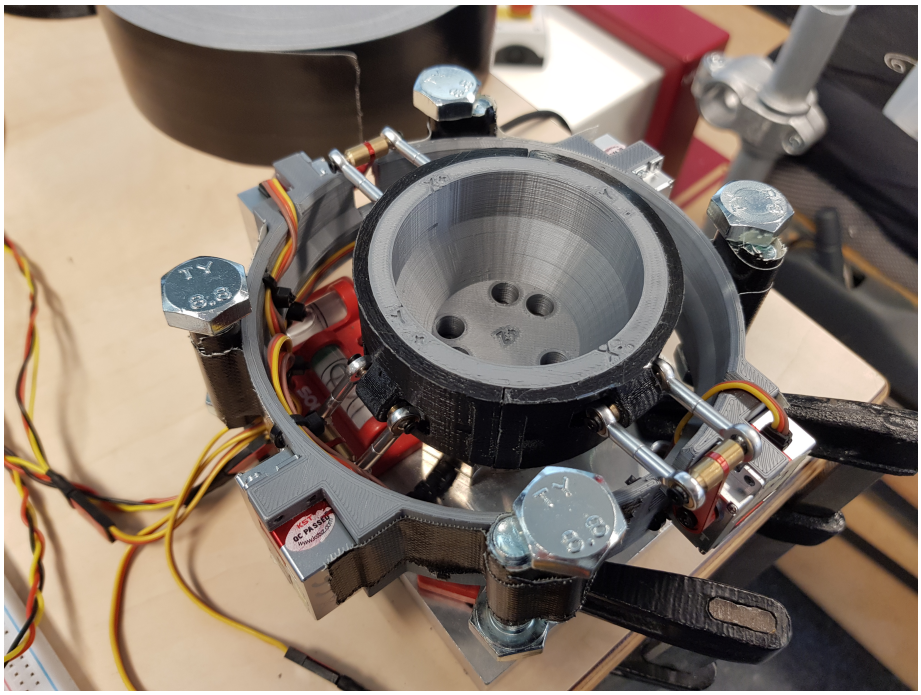

Figure 6.35: Bolts used to increase the moving mass

mass of 0.25kg and the motors that are able to provide ample torque to generate such a signal.

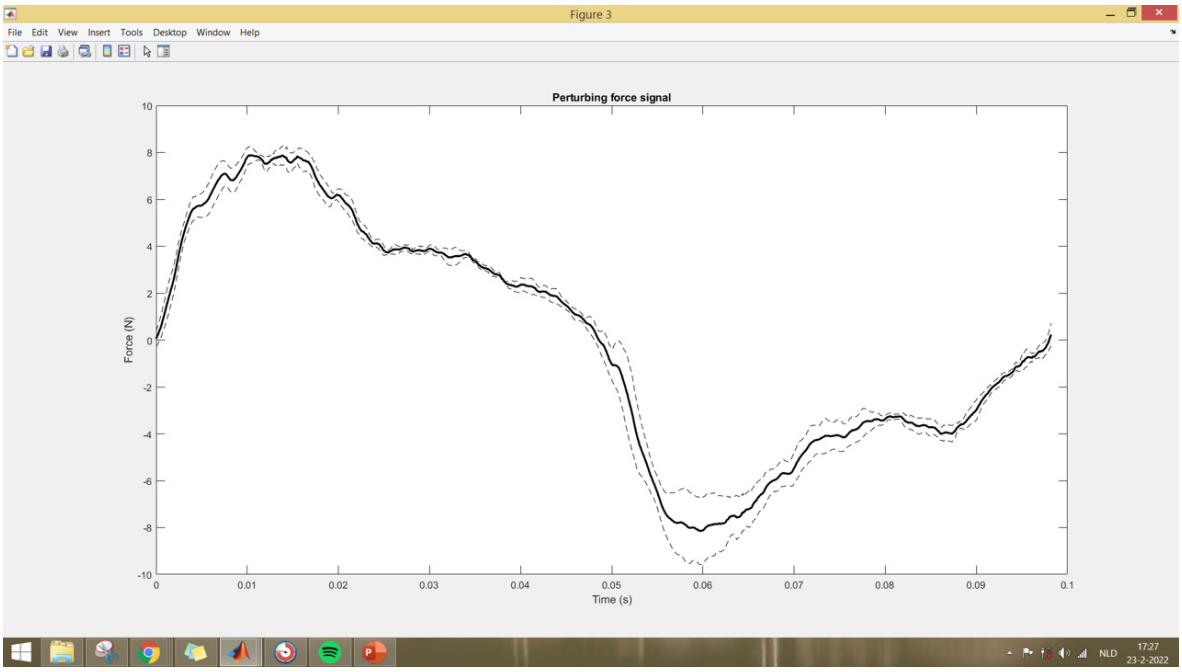

Figure 6.36: Smooth 8N perturbation achieved with 0.25g added weight